CARBON-SUPPORTED PT NANOPARTICLES PREPARED BY NEW SURFACTANTS AND DIFFERENT REDUCING AGENTS FOR METHANOL OXIDATION REACTION

A THESIS SUBMITTED TO
THE GRADUATE SCHOOL OF NATURAL AND APPLIED SCIENCES
OF
MIDDLE EAST TECHNICAL UNIVERSITY

BY

SEVDA KALYONCU

IN PARTIAL FULFILLMENT OF THE REQUIREMENTS
FOR
THE DEGREE OF MASTER OF SCIENCE
IN
CHEMISTRY

APRIL 2015

Approval of the thesis:

CARBON-SUPPORTED PLATINUM NANOPARTICLES PREPARED BY NEW SURFACTANTS AND DIFFERENT REDUCING AGENTS FOR METHANOL OXIDATION REACTION

Submitted by **SEVDA KALYONCU** in partial fulfillment of the requirements for the degree of **Master of Science in Chemistry Department, Middle East Technical University** by,

Prof. Dr. Gülbin Dural Ünver
Dean, Graduate School of **Natural and Applied Sciences** _____

Prof. Dr. İlker Özkan
Head of Department, **Chemistry** _____

Prof. Dr. Gülsün Gökağaç
Supervisor, **Chemistry Dept., METU** _____

Examining Committee Members:

Prof. Dr. Ceyhan Kayran
Chemistry Dept., METU _____

Prof. Dr. Gülsün Gökağaç
Chemistry Dept., METU _____

Assoc. Prof. Dr. Metin Aydın
Chemistry Dept., OMU _____

Assoc. Prof. Dr. Ayşen Yılmaz
Chemistry Dept., METU _____

Assist. Prof. Dr. Emren Nalbant Esentürk
Chemistry Dept., METU _____

Date: 27.04.2015

I hereby declare that all information in this document has been obtained and presented in accordance with academic rules and ethical conduct. I also declare that, as required by these rules and conduct, I have fully cited and referenced all materials and results that are not original to this work.

Name, Last name: Sevda Kalyoncu

Signature:

ABSTRACT

CARBON-SUPPORTED PT NANOPARTICLES PREPARED BY NEW SURFACTANTS AND DIFFERENT REDUCING AGENTS FOR METHANOL OXIDATION REACTION

Kalyoncu, Sevda

M.S., Department of Chemistry

Supervisor: Assoc. Prof. Dr. Gülsün Gökağaç

April 2015, 53 pages

In this thesis, carbon supported platinum catalysts were synthesized to investigate the effect of reducing agent and surfactant on the performance of catalyst towards methanol oxidation reaction. For this purpose, the catalysts were prepared by using $PtCl_4$ as a starting material, propylamine (a) and dipropylamine (b) as surfactant, and sodium borohydride (catalyst I) and formaldehyde (catalyst II) as reducing agent. The prepared catalysts were characterized by X-ray diffraction (XRD), transmission electron microscopy (TEM), X-ray photoelectron spectroscopy (XPS), Fourier transform infrared spectroscopy (FTIR), Brunauer–Emmett–Teller (BET) surface area analysis, cyclic voltammetry (CV) and chronoamperometry (CA).

XRD and TEM results indicated that platinum has face-centered cubic (fcc) structure and it consists of small (~5nm) and agglomerated (30-70 nm for catalyst I, 40-120 nm for catalyst II) particles and they were homogeneously dispersed on carbon support. The results also revealed that the morphology of the platinum particles depends on the kind of reducing agent, for instance; they have cubic and formless shape when sodium borohydride and formaldehyde were used, respectively.

The Pt 4f region of XP spectra showed that platinum has two different oxidation states, Pt(0) and Pt(IV), and it composed of 61-67 % Pt (0) and 39-33 % Pt(IV).

Oxygen 1s and carbon 1s peaks displayed that there are CO_{ads}, OH_{ads}, H_2O_{ads}, $(C=C)_{ads}$, $(C-O)_{ads}$, $(C=O)_{ads}$ and $(COO^-)_{ads}$ on the surface of catalyst.
BET analysis revealed that the surface areas of the catalyst Ia-b and IIa-b before adding carbon support were ~49 m^2/g sample and ~32 m^2/g sample, respectively.

Electrochemical studies indicated that;

a) The performance of catalysts depends on the kind of surfactants and reducing agents.

b) Catalyst Ia has the best performance towards methanol oxidation reaction, because it has highest electrochemical surface area, percent platinum utility and roughness factor.

c) The performance of catalyst Ia (~240 mA/mg Pt) is ~3 times larger than commercial E-TEK catalyst (~75 mA/mg Pt).

Keywords: Direct Methanol Fuel Cells, Platinum Nanoparticles, Carbon-Supported Catalysts, Cyclic Voltammetry, X-ray Diffraction, Transmission Electron Microscopy, X-ray Photoelectron Spectroscopy

ÖZ

METANOL YÜKSELTGENME TEPKİMESİ İÇİN YENİ SÜRFAKTANLAR VE DEĞİŞİK İNDİRGEYİCİLER KULLANARAK KARBON DESTEKLİ PT NANOPARÇACIKLARININ HAZIRLANMASI

Kalyoncu, Sevda
Yüksek Lisans, Kimya Bölümü
Tez yöneticisi: Prof. Dr. Gülsün Gökağaç

Nisan 2015, 53 sayfa

Bu çalışmada, katalizörün metanol yükseltgenme tepkimesine karşı performansına indirgeyici ve sürfaktanın etkisini araştırmak için karbon destekli platin katalizörler sentezlendi. Bu amaçla, başlangıç maddesi olarak $PtCl_4$, sürfaktan olarak propilamin (a) ve dipropilamin (b), indirgeyici madde olarak sodyum borhidrür (katalizör I) ve formaldehit (katalizör II) kullanılarak katalizörler hazırlandı. Hazırlanılan katalizörler, X-ışınları kırınımı (XRD), geçirmeli electron mikroskobu (TEM), X-ışınları fotoelektron spektroskopisi (XPS), Fourier dönüşümlü kızılötesi spektroskopisi (FTIR), Brunauer–Emmett–Teller (BET) yüzey analizi, dönüşümlü voltametri (CV) ve kronoamperometri (CA) ile karakterize edildi.

XRD ve TEM sonuçları platinin yüzey-merkezli kübik yapıya sahip olduğunu ve küçük (~5nm) ve aglomere (katalizör I için 30-70 nm, katalizör için 40-120 nm) parçacıklardan oluştuğunu ve karbon destek üzerinde homojen bir şekilde dağıldığını gösterdi. Sonuçlar ayrıca göre platin parçacıklarının morfolojisinin indirgeyici maddeye bağlı oldu gösterdi, örneğin; platin parçacıkları sodyum borhidrür kullanıldığında kübik, formaldehit kullanıldığında ise biçimsiz şekle sahiptir.
X ışını fotoelektron spektrumunun Pt 4f bölgesi platinin iki farklı yükseltgenme basamağı olduğunu, Pt(0) ve Pt(IV), ve 61-67 % Pt(0) ve 39-33 % Pt(IV)'ten

oluştuğunu gösterdi. Oksijen 1s ve karbon 1s piklerin katalizörün yüzeyinde CO_{ads}, OH_{ads}, H_2O_{ads}, $(C=C)_{ads}$, $(C-O)_{ads}$, $(C=O)_{ads}$ ve $(COO^-)_{ads}$ olduğunu gösterdi.

BET analizlerine göre karbon eklemeden önceki katalizör Ia-b ve IIa-b'nin yüzey alanları sırasıyla ~49 m^2/g madde ve ~32 m^2/g madde bulundu.

Elektrokimyasal çalışmalar aşağıdaki sonuçları gösterdi;

a) Katalizörlerin performansları sürfaktan ve indirgeyicilerin çeşidine bağlıdır.

b) Katalizör Ia metanol yükseltgenme reaksiyonuna karşı en iyi performansa sahiptir, çünkü bu katalizör en yüksek elektrokimyasal yüzey alanına, yüzde platin verimine ve pürüzlük faktörüne sahiptir.
c) Katalizör Ia'nın performansı (~240 mA/mg Pt) ticari E-TEK katalizöründen (~75 mA/mg Pt) 3 kat daha büyüktür.

Anahtar Kelimeler: Doğrudan Methanol Yakıt Pilleri, Platin Nanoparçacıkları, Karbon-Destekli Platin Katalizörleri, Dönüşümlü Voltametre, X-ışınları Kırınımı, Geçirmeli Elektron Mikroskobu, X-ışınları Fotoelektron Spektroskopisi

To my mum,

ACKNOWLEDGEMENTS

First of all, I would like to express my deep gratitude to my supervisor Prof. Dr. Gülsün Gökağaç for giving me a chance to study on a very hot topic in a well-equipped laboratory. Her endless support, encouragement, patience, logical criticism with her wide knowledge through this thesis have been very precious for me.

I owe many thanks to Assoc. Prof. Dr. Ayşen Yılmaz for her kindness and help about XRD measurement.

I want to thank to Dr. Fatih Şen for his guidance at the beginning of the research.

I would like to thank to all my lab partners; Aysu Aslantürk who is always my best friend and stand behind me with her lovely support since 2001, Deniz Çakal, and Seda Ergan for all the support and very precious, cheerful times we spent together.

I owe many many thanks to Sevinç Aslantürk for her endless support, homemade foods and special love.

I would like to thank TÜBİTAK for financial support (project number:111T162).

I want to thank METU Central Lab. for all the measurements and I owe many thanks to METU Chemistry Department for giving me the chance of having MS education with the sophisticated proffessors and studying in the well-equipped laboratories.

Finally, I gratefully thank to my mum for her endless support, encouragement and precious love.

TABLE OF CONTENTS

LIST OF TABLES

TABLES

LIST OF FIGURES

FIGURES

CHAPTER 1

INTRODUCTION

1.1. ENERGY NEED AND FUEL CELLS

One of major requirements for living organism is the energy. Today the aims of using energy is for electricity, heat engine and transportation. Energy resources can be classified as renewable and nonrenewable. Renewable energy is the energy which is produced by using natural sources which are sun, wind and so on, where nonrenewable energy is the energy which is generated from fossil fuels like natural gas, oil and coal. Most of the energy need is supplied from the nonrenewable ones[1].

In recent decades development of technology, industry and also increase in the population cause extreme consumption of energy all over the world. Most of the energy used in common acquired from fossil fuels. However, depletion of fossil fuels and the environmental population increase demands on new sources. Most important reason of this demand is that the emissions from fossil fuels like SO_2 (sulphur dioxide), NOx (Nitrogen oxide groups), CO (carbon monoxide), PAH (polyaromatic hydrocarbons), benzene, HC (hydrocarbons), CO_2 (carbon dioxide) and the results of such pollution which causes smog, acid rain, ruining the ecologycal balance and also affecting the human health badly, especially in large cities. Thus, researchers tend to find new energy sources like solar, wind, biomass, power plants and different renewable sources. Fuel cell is one of these sources that supplies clean, efficient and reliable power generation for lots of electrical device [1,2].

A fuel cell is a device that directly converting the chemical energy of a fuel into the electrical energy throughout the chemical reactions to produce electricity. Each fuel cell consists of three adjacent segments which are anode, cathode and

electrolyte/membrane. In these system, a catalyst is needed to accelerate the chemical reactions take place at anode and cathode. On the anode side fuel is oxidized, while on the cathode side oxygen is reduced. At this point, the electrolyte transports charged particles between the electrodes and it is thought that it must permit only proper ions between anode and cathode. If any other free electrons or species travel through the electrolyte, they would hinder the chemical reaction. Therefore, electrolyte should be chosen conscientiously [3].

1.2. HISTORY OF FUEL CELLS

In 1791, Luigi Galvani who is an Italian physiologist defined a new phenomenon which is known as “galvanic phenomena” or “galvanism” by performing an interesting experiment that the muscles of a frog’s leg contracts each time the nerve and the muscle is connected with two different metals. Alessandro Guiseppe Antonio Anastasio Volta, one of the enthusiasts of Galvani, repeated Galvani's frog experiments many times with different materials and he found that it was not the leg of frog which generates electricity, the reason was the two unlike metals. After several experiments, in March 1800, Volta invented “voltaic pile” that provides enduring electrical charge. With this progress, important developments were achieved on the fields of electricity and electrochemistry and lots of electrochemical process were analyzed in a short period [3-7].

In 1802, William Nicholson and Sir Anthony Carlisle performed the electrolysis of water that results with the production of hydrogen and oxygen. By following this achievement, a British lawyer, judge and physical scientist Sir William Robert Grove performed a series of experiments regarding electrolysis of water and he designed a cell illustrated in Figure 1.1 which comprises of two platinum electrodes immersed in an acidified water (by sulfuric acid) [8]. He considered that if water can be decomposed into the hydrogen and oxygen by a current pass, so the opposite reaction may also come true and energy can be produced by this way. Therefore, he disconnected the current and observed that when hydrogen and oxygen were supplied to both of platinum electrodes connected to an external circuit, a constant current

flow was occurred in this circuit. This creation was called as “gas battery” or “gas voltaic battery” which is thought to be the first archetype of a fuel cell [5-7].

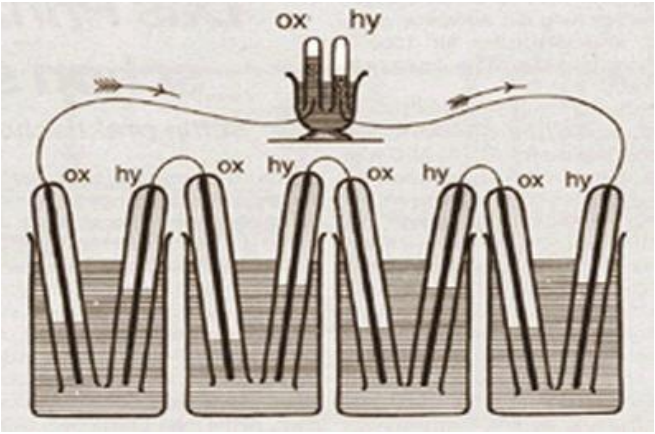

Figure 1.1. Sir William Robert Grove’s cell [7].

In 1889, Ludwig Mond and his assister Carl Langer was first to use the term “fuel cell”. They designed a hydrogen-oxygen fuel cell using air and industrial coal gas also called Mond gas. They got 6 amps per square foot (measuring electrode’s surface area) at 73 volts. Mond and Langer used thin, perforated platinum electrodes. In order to solve Grove’s electrolyte problem, they built a diaphragm to keep sulfuric acid and prevent electrode flooding. However, reproducibility and performance problems made their research non-applicable in practical. After Mond and Langer, a German scientist Friedrich Wilhelm Ostwald, experimentally identified the relationship between the different components of the fuel cell which are electrodes, electrolyte, oxidizing and reducing agent, anions and cations. Moreover, Ostwald presented an idea of converting the chemical energy of natural fuels directly to the electrical energy based on thermodynamics [3-7].

In 1896, William Jacques had invented a process of generating electricity directly from coal. Jacques built a 1.5 kW fuel cell where a carbon electrode reacts with an alkali electrode that the air was injected into it. However, in 1904, Haber and Bruner made an interpretation on Jacques’ cell was actually a hydrogen-oxygen fuel cell in one sense that hydrogen was generated with a chemical reaction between carbon and

sodium hydroxide. In 1913, Siegl achieved to reduce the cost of electrodes by dopping platinum onto the carbon support. Then, Muller worked on the electrooxidation of organic fuels on different metals. In the early 20th century, Emil Baur carried out an extensive research of high temperature fuel cells which used molten silver as the electrolyte [3-10].

Just after the studies of Baur and co-workers, Baur and Brunner carried out a research concentrated on the enhancement of fuel cells. They claimed that the presence of CO_2 (carbon dioxide) in the cathode provides a better performance. Furthermore to Baur's work, Oganes Davtyan worked on fuel cells with the aim of using a highly conducting and more stable electrolyte. For this purpose, Davtyan designed a fuel cell which oxidized CO with air at 700 °C and could operate for days. He also studied on low temperature hydrogen-oxygen fuel cells and wrote a book about all his researches that he carried out. That book was published in 1947 have an importance due to the fact that it was the first book about fuel cells around the world.[3-10].

In 1932, Francis Thomas Bacon improved early Mond-Langer fuel cell by changing the acidic electrolyte solution (sulfuric acid) with the alkaline one (KOH). With the improvements of strentgth of this fuel cell, "Bacon Cell" is developed [5].

Grubb, while working for General Electric (GE) as a chemist, made a major advance in fuel cells, originally designed by Sir William Grove in 1839 by development of the sulphonated polystyrene ion-exchange membrane in 1955 (Proton Exchange Membrane Fuel Cell). After three years, another GE chemist, Leonard Niedrach, found a way to deposit platinum on that membrane. The improvements done by Grubb and Niedrach named as "Grubb-Niedrach fuel cell". Thus, Grubb and Niedrach succeed that in fuel cells hydrocarbons (methane,ethane etc) could be electrochemically oxidized by using platinum catalysts below 150 °C. This showed that direct conversion of chemical energy of a natural fuel into the electrical energy is possible. In 1960s, National Aeronautics and Space Administration (NASA), the

US government agency, were searching a new way to power the manned space flights. Applicable energy resources like batteries, solar energy and nuclear energy had many challenges for this flights. Therefore, NASA got sponsorships to develop an applicable fuel cell for spacecrafts due to that fuel cells was a good alternative energy. In 1962, GE and NASA used the fuel cell in Gemini space project and this was the first commercial use of a fuel cell. Pratt & Whitney's company got license to work on Bacon's patent and improved it in 1960 and they used that fuel cell for Apollo spacecraft program. In these years, while the researchers showed great interest to enhance the fuel cells for space applications, the earth applications had nearly no improvement [5].

The oil crisis in 1973 led to an increase in the interest to the fuel cells for earth applications, in order to reduce the dependence on petroleum products. Lots of companies began to search new ways to optimize the fuel cells and reduce the high cost for widespread commercialisation. Through the 1980s, fuel cell technology was started to use in automobile sector and a Canadian company, Ballard, brought the first vehicle powered by fuel cell out in 1993. So, using fields of fuel cells are began to expand gradually due to their advantages compared to other resources. The important developments in fuel cell history is given in Figure 1.2 [10].

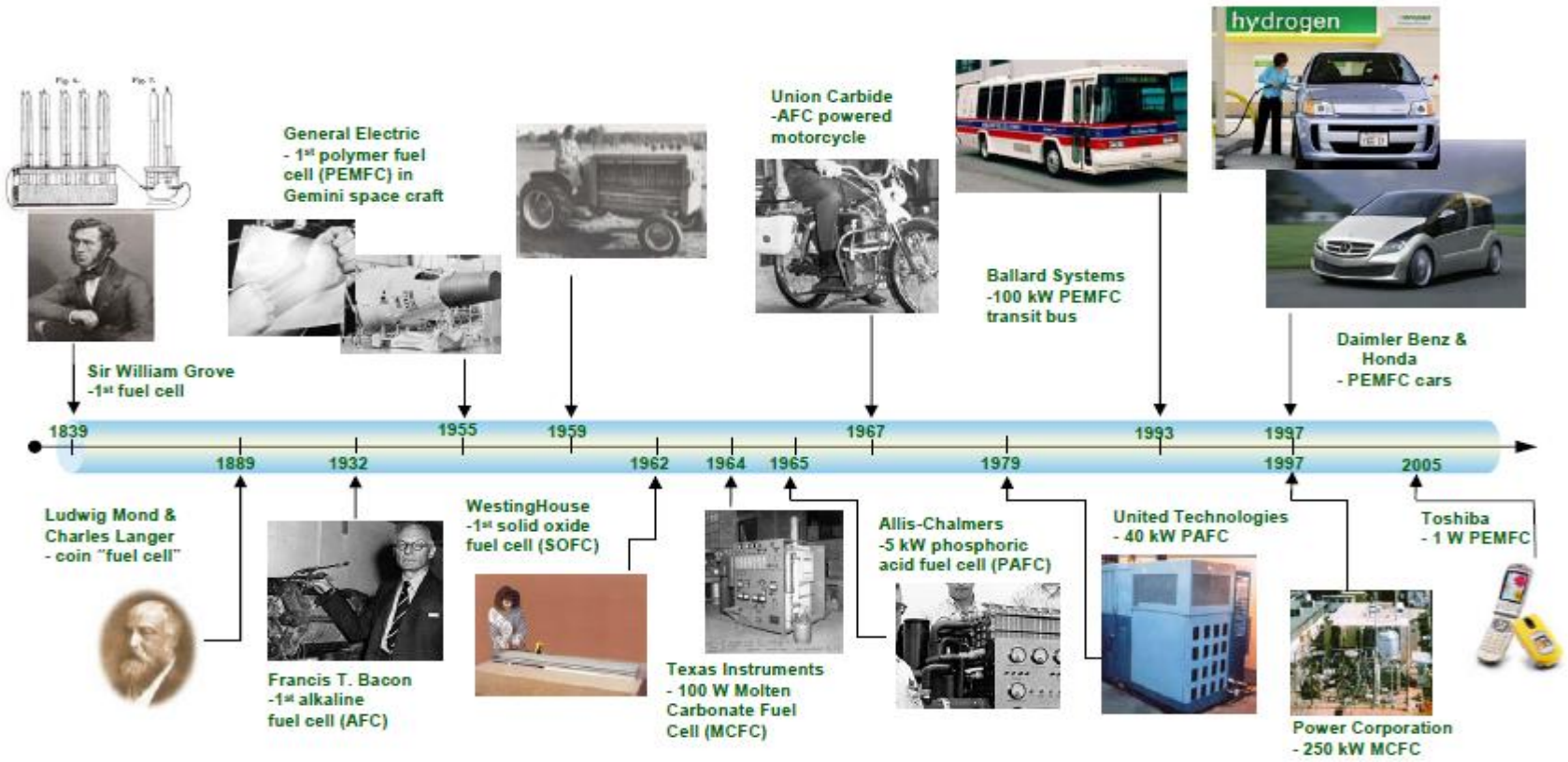

Figure 1.2. Fuel cell history [11].

1.3. APPLICATIONS OF FUEL CELLS

Use of fuel cells could be categorised into three broad areas: stationary power generation, power for transportation and portable power generation. Stationary fuel cells are the largest, most powerful fuel cells. Due to their advantages that they are noiseless, environmentally friendly and efficient fuel cells supply power to hospitals, banks, airports, schools, homes and so on. As an example; fuel cells already provide a power supply to lots of homes in Japan and this is beginning to do in the United States, too. Fuel cell buses and cars can significantly reduce greenhouse gas emissions when compared to other conventional technologies. So the increasing demand to end the dependence on petroleum, fuel cell-powered cars and busses are most likely to be used extensively. Fuel cells can power any portable device or machine which works with batteries. However; while batteries ultimately run down, fuel cells maintain to generate electricity as long as fuel and oxidant are supplied. Mobile phones, laptops, video recorders are some of portables that could be powered by fuel cells [5,7,8,12]

1.4. TYPES OF FUEL CELLS

Each of fuel cell types differ in characteristics, advantages and disadvantages. The classification of fuel cells provides knowledge about that which chemical reactions occur in fuel cell, what kind of catalyst and fuel is used, which temperature range is optimum for operation and so on. Moreover, according to these properties researchers decide in which applications the cells are most suitable. Fuel cells are categorized according to electrolyte type that is employed, the main types can be grouped as; polymer electrolyte membrane fuel cell (PEMFC), alkaline fuel cell (AFC), phosphoric acid fuel cell (PAFC), solid-oxide fuel cell (SOFC) and molten carbonate fuel cell (MCFC). Several variety of fuel cells like direct methanol fuel cells (DMFC) considered to be a kind of PEMFC are studied and researchers keep on improving fuel cell technologies by using brand new catalysts and electrolytes to improve the performance and decrease the cost for commercial use and microbial fuel cell is one of them. The operating properties, the advantages and the applications of the major types of fuel cell (and also DMFC) are given in Table 1.1 [5,7,12,13].

1.5. DIRECT METHANOL FUEL CELL AND ITS ADVANTAGES

DMFC is a subcategory of PEMFC. Similar to polymer electrolyte membrane (PEM) fuel cells powered directly by hydrogen or by reforming hydrogen, in DMFCs liquid methanol is used as a fuel that is oxidized directly at the anode side and oxygen in the air is reduced at the cathode side. Thus, no hydrogen reformer or storage tank is required for a DMFC and that makes DMFC systems a highly promising alternative energy resource.

In recent decades, DMFCs have drew more attention by the scientists and companies. On the grounds that direct methanol fuel cells offers a number of advantages [17,18], including:

- In DMFCs, liquid methanol which is an organic liquid is used as fuel that has a higher energy density ($d_{methanol}$= ~16 MJ/L) compared to hydrogen gas' ($d_{hydrogen}$= 9 MJ/L).
- Moreover, methanol is relatively cheap, thus it can be easily handled and also readily available from fossil fuels, wood or fermentation of agricultural waste.
- Methanol is reactive at low temperatures and soluble in aqueous electrolytes which make the operating properties optimum in labs.
- Methanol is also easy to store and transport.
- DMFCs have a comparatively simpler system design which has no moving part, with the potential for low-volume and lightweight packaging.
- Unlike batteries there is no memory effect in fuel cells.
- In DMFCs, no combustion occurs during the operation (so there are no harmful products such as SO_2, NO_2, soot and soon.
- In DMFCs, operation is silent.
- DMFCs have adjustable size and shape.

- DMFCs can be classified as environmentally friendly zero emission power due to the absence of toxic byproducts except for CO_2 which is a green house gas. Although relatively small amount of carbon dioxide is evolved at the end of reactions, there is no combustion as in heat engines that use fossil fuels, so there is no byproducts like sulfur or nitrogen oxides.

All these advantages increase the demand to use DMFCs in commercial life. Direct methanol fuel cells especially can be seen as one of the most effective fuel cell system for the use in portable applications such as mobile phones, laptops, cameras due to the small size, high efficiency, high dense energy of methanol, fast refueling and capacity of refueling during the operation. DMFCs can be not only used in portable devices, but also used in some electrical vehicles and stationary power plants.

Table 1.1. The type, electrolyte, operating temperature, efficiencies and applications of fuel cells.

Fuel Cell Type	Common Electrolyte	Operating Temperature	Electrical Efficiency	Combined Heat and Power Efficiency (CHP)	Applications
Polymer Electroyte Membrane(PEM)	Solid organic polymer Poly-perfluorosulfonic acid	50-100 ºC	53- 58 % (transportation) 25- 35 % (stationary)	70-90 % (low grade waste heat)	-Backup power -Portable power -Transportation
Alkaline (AFC)	Aqueous solution of potassium hydroxide soaked in a matrix	90-100 ºC	60 %	> 80 % (low grade waste heat)	-Military -Space
Phosphoric Acid (PAFC)	Liquid sulfuric acid soaked in a matrix	150-200 ºC	> 40 %	> 85 %	-Distributed generation
Molten Carbonate (MCFC)	Liquid solution of lithium,sodium and/or potassium carbonates soaked in a matrix	600-700 ºC	45-47 %	> 80 %	-Power company
Solid Oxide (SOFC)	Yttria stabilized zirconia	600-1000 ºC	35-43 %	< 90 %	-Auxiliary power -Power company -Large distributed generation
Direct Methanol (DMFC)	Solid organic polymer Poly-perfluorosulfonic acid	50-100 ºC	20-25 %	70-90 %	-Portable -Mobile

In direct methanol fuel cells, there are three segments anode, cathode and membrane. A representation of a DMFC is shown in Figure 1.3. In anode side, the fuel which is methanol is oxidized to carbon dioxide and in cathode side, oxygen is reduced to water [6,7,9]. The reactions for methanol oxidations are [5];

Anode reaction:

$CH_3OH + H_2O \rightarrow 6\,H^+ + 6\,e^- + CO_2$ $\quad E^0 = 0.02$ V (vs. SHE)

Cathode reaction:

$3/2\,O_2 + 6\,H^+ + 6\,e^- \rightarrow 3H_2O$ $\quad E^0 = 1.23$ V (vs. SHE)

Overall reaction:

$CH_3OH + 3/2\,O_2 \rightarrow CO_2 + 2H_2O$ $\quad E^0 = 1.21$ V (vs. SHE)

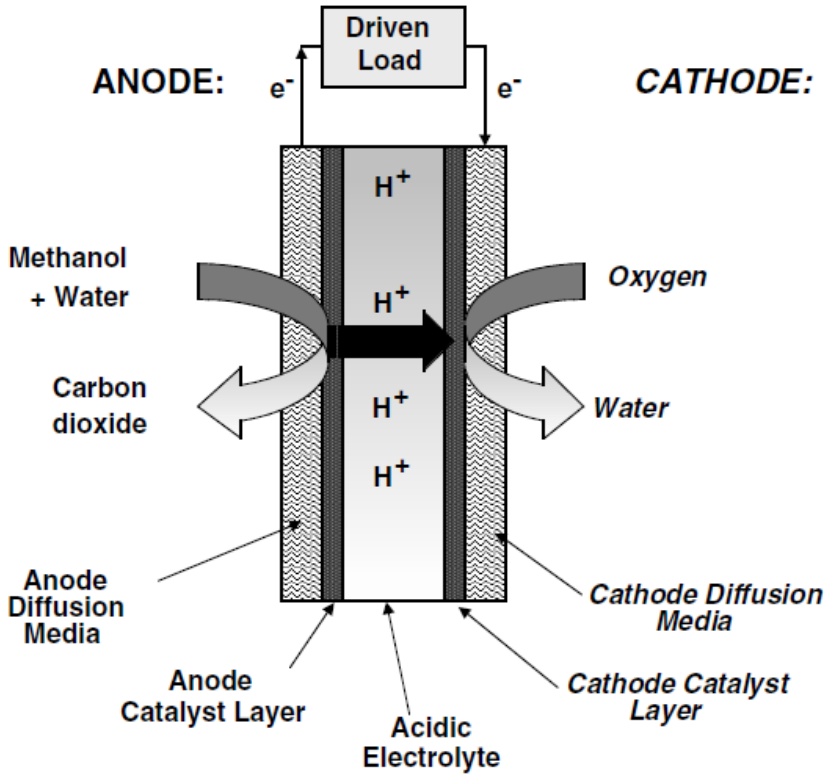

Figure 1.3. Schematic representation of DMFC with acidic electrolyte [7].

In DMFC, principal products are carbon dioxide and water at all. In addition to this principal products; some byproducts are also formed in small amounts, because methanol oxidation comprises a few steps. Firstly, methanol is dehydrogenated;

$$CH_3OH \rightarrow COH_{ads} + 3\,H_{ads}$$

$$3\,H_{ads} \leftrightarrow 3\,H^+ + 3\,e^-$$

After dehydrogenation of methanol into COH_{ads}, oxidation of these species occurs with H_2O_{ads} or OH_{ads} and as consequence CO_2, H^+ and electrons are produced.

$$COH_{ads} + H_2O_{ads} \text{ (or } OH_{ads}) \rightarrow CO_2 + 3\,H^+ + 3\,e^-$$

However, there is a possibility of the adsorption of carbonyl (CO) onto the catalyst surface instead of CO_2 production and that causes poisoning of the catalyst surface. In this circumstance, methanol electrosorption is prevented and methanol oxidation reaction can not take place. This is called poisoning of the catalyst. All the adsorption of methanol process and poisoning occurance are shown in Figure 1.4 [9].

Although DMFCs have great advantages among the other fuel cells, the development of commercial DMFCs has been limited by some important reasons. In order to achieve rising up the use of DMFCs in commercial, some enhancements must be succeed such as:

- To achieve studying at higher temperatures, an innovative membrane should be developed in order to reach a fine settlement between conductivity, methanol cross-over, mechanical and thermal stability.
- Life time of DMFCs should be improved.
- Some precautions should be developed to prevent the poisoning of catalysts.

Besides these enhancement, the rate of methanol oxidation reaction should also be increased, for this purpose the new anode catalyst materials which are noble and

nonnoble metals should be explored or new carbon supported Pt-alloy catalysts should be developed as possible as in lower price in order to use DMFCs commonly in daily life and to increase the efficiency of DMFCs [14,15].

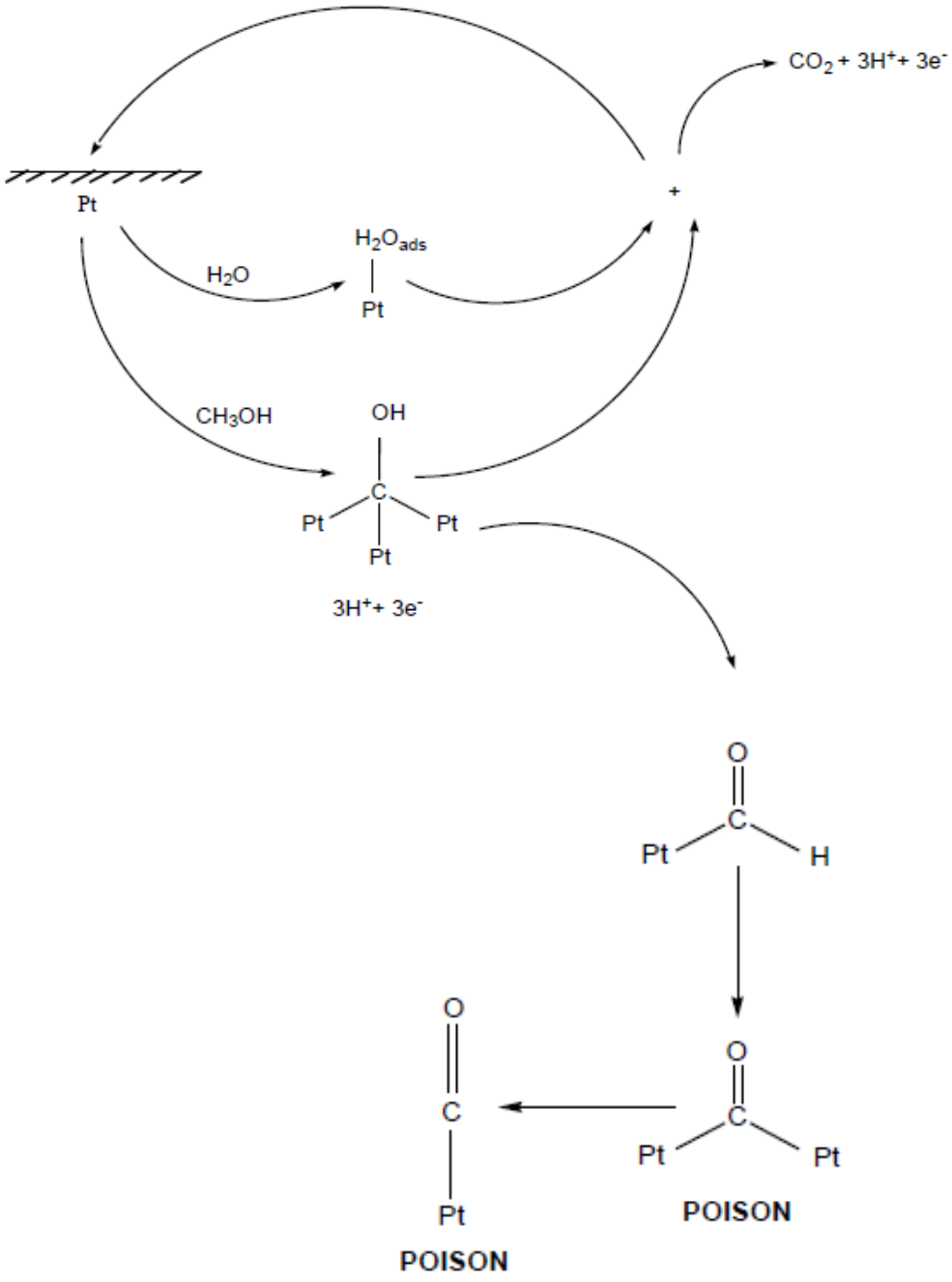

Figure 1.4. Schematic diagram of methanol oxidation taking place on the platinum catalyst surface and the poisoning [9].

1.5. THE NEED FOR CATALYST

As mentioned above, eventhough methanol has various advantages on direct methanol fuel cells, it has a drawback which is methanol shows poor electrochemical reactivity in acidic solutions. Thus, a catalyst is needed to activate methanol. According to all researches carried out to find an efficient catalyst, platinum or platinum-based nanomaterials are still indispensable and most efficient catalyst for methanol activation in fuel cells. Platinum which is a valuable transition metal has extraordinary catalytic and electrical properties and resistant to corrosion. However, there is a handicap of platinum that it is a high cost and rapidly poisoning metal. Therefore, the scientists have been trying to develop more efficient and low cost catalyst for methanol electrooxidation in acidic solution in order to use direct methanol fuel cells more practically applicable [5-17].

1.6. NANOPARTICLE CONCEPT

Nanoparticles are defined as particles with a size between 1-100 nm (1 nm = 10^{-9} m). According to the preparation procedure, nanoparticles or nanospheres or nanocapsules can be acquired. In recent years, nanoscience which is also manipulation of matter at the atomic and molecular scale have been popular due to new technologies in sample preparation and fabrication of devices. A great deal of researches have been done in a wide range of fields by physicist, chemists, material scientists and mechanical and electrical engineers. Eventually, a lot of glamorous and challenging results were developed that lead researchers' perspective understanding of quantum phase transition, surface effect and etc. Thus, nanotechnology now have a wide variety of applications in biomedical, optical, and electronic fields [18].

Most of physical and mechanical properties of nanoparticles changes due to the size reduction (e.g. lower melting points, higher active surface areas, enhanced optical properties) and this alteration makes the nanosized particles different from bulk materials. Nobel metal nanoparticles which have attractive size-dependent properties as electrical, optical, magnetic and chemical have been drew attention due to their technological applications [5-18].

In DMFCs, to achieve greater catalytic activity, platinum nanoparticles were used to prepare catalysts. When the size is reduced into the nanometer scale, active surface area is increased more and the higher activity is provided with the higher active surface area. Thus, studying at nanoscale provided to get high activity results towards to methanol oxidation. In this study, approximately 5 nm-sized particles were synthesized. In previous studies, 2-3 nm sized particles were also observed, but surfactants, operating conditions differs from this study [19,20].

1.7. THE AIM OF STUDY

Fuel cells are very promising future energy resource and direct methanol fuel cell (DMFC) is one of the most attractive ones providing various advantages given before. Despite all the advantages, there is a drawback with DMFC. Methanol has poor electrochemical activity which prevents the commercial use. In order to overcome this problem, a catalyst is needed and anormous number of catalysts have been prepared, but they do not have enough performance and low cost to use in daily life. Therefore, in this study, new types of catalysts have been synthesized to enhance performance and to define the effect of surfactants and reducing agents on the activity of catalysts. For this purpose, carbon-supported Pt nanoparticles were prepared by using $PtCl_4$ as starting material, propylamine and dipropylamine as surfactants, formaldehyde and sodiumborohydride as reducing agents for methanol oxidation reaction. The prepared catalysts have been characterized by transmission electron microscopy (TEM), X-ray diffraction (XRD), X-ray photoelectron spectroscopy (XPS), Fourier transform infrared spectroscopy (FTIR), induced coupled plasma (ICP) analysis, Branauer-Emmett-Teller (BET) surface area analysis, cyclic voltammetry (CV) and chronoamperometry (CA).

CHAPTER 2

EXPERIMENTAL

2.1. CHEMICALS

$PtCl_4$ (99 %) was obtained from Alfa, formaldehyde (37 %), $NaBH_4$ (96 %), toluene (99 %), NaOH (99 %), ethanol (99.2 %), methanol (99.8 %), N,N-dimethyl formamide (99.8 %), HClO4 (60 %) was purchased from Merck, dipropylamine (99 %), nafion (5 %) were brought from Sigma-Aldrich, propylamine (99 %) was acquired from SAFC and Vulcan Carbon (XC-72) was obtained from Cabot Europa Ltd. All chemicals in this study were of analytical grade purity. Distilled water was purified with Millipore water purification system (18 MΩ) analytical grade. All the glassware were washed with distilled water repeatedly and dried in the oven.

2.2. SYNTHESIS OF CATALYSTS

2.2.1. SYNTHESIS OF CATALYST Ia

0.24 mmol (0.0808 g) of $PtCl_4$ was dissolved in 120 mL deionized water and yellowish solution was stirred for 20 minutes vigorously. Then, 2.4 mL of 0.112 M $NaBH_4$ as reducing agent was added dropwise to the solution. Reduction of Pt(IV) to Pt(0) was observed by the change of color of the solution from yellowish to black. After that, 0.24 mmol (20 μL) of propylamine as surfactant was dissolved in 120 mL of toluene and put into the black solution. When the addition was completed, two phases occured. Upper phase was toluene-consisting phase and lower phase was watery phase. Platinum nanoparticles were observed between these phases. Later, 1.4 mL of 1.0 M NaOH was added into the solution in order to get better phase separation and mixture was stirred for 2 hours in a closed system under Ar gas. Then, the phases were separated by the help of separation funnel. After the separation, platinum nanoparticles which occured at intermediate phase were taken into the centrifugate tubes and washing process was applied. To remove excess amines, final solution was washed by dry ethanol and held in ultrasonic bath for 5 minutes and

centrifugated for seven times. After the precipitation, platinum nanoparticles were dried under vacuum at room temperature.

2.2.2. SYTHESIS OF CATALYST IIa

0.24 mmol (0.0808 g) of $PtCl_4$ was dissolved in 120 mL deionized water by stirring for 20 minutes 0.48 mmol (36 μL) of formaldehyde solution was added after stabilizing temperature to 75°C and pH of the solution to 9 by using 2.5 M NaOH in order to achieve better reduction. The color change of solution from yellowish to black shows the generation of reduced platinum nanoparticles. After a few minutes, 0.24 mmol (20 μL) of propylamine dissolved in 120 mL toluene was added as surfactant. Then, 1.4 mL of 1.0 M NaOH was added to the mixture for better separation and then solution was stirred for 2 hours. All these process was carried out under argon gas. After stirring, there were two phases as toluene-consisting (upper) and watery (lower) phase, and between these phases platinum nanoparticles were accumulated. The separation of the mixture was achieved with the separatory funnel and platinum nanoparticles were washed seven times by sonicating with dry ethanol and centrifugating for 10 minutes to remove the excess amines caused by surfactant. Then, these platinum nanoparticles were dried under vacuum at room temperature.

2.2.3. SYNTHESIS OF OTHER CATALYSTS

The appropriate amounts of $PtCl_4$ were also used as starting material in the synthesis of catalyst Ib and IIb. All the experimental processes were the same for all of the catalyst except the ingredients. For catalyst Ib, platinum nanoparticles were reduced by $NaBH_4$ by following the same procedure as explained in section 2.1.1. For catalyst IIb, formaldehyde solution was used as reducing agent and the same procedure as in section 2.1.2 was carried out. Dipropylamine used as surfactant for both catalyst Ib and IIb to stabilize platinum nanoparticles (Table 2.1).

Table 2.1. The name of catalysts, reducing agents and surfactants.

Catalysts	**Reducing agents**	**Surfactants**
Cat Ia Cat Ib	Sodium borohydride	Propylamine Dipropylamine
Cat IIa Cat IIb	Formaldehyde	Propylamine Dipropylamine

2.2.4. PREPARATION OF CARBON SUPPORTED PLATINUM NANOPARTICLE CATALYST

The synthesized Pt nanoparticles were mixed with Cabot Vulcan XC-72 carbon black as supporting material with a ratio of 1:9, respectively.. Then, 10 mL of dry ethanol was introduced into the mixture and it was stirred in ultrasonic bath for 3 days to get uniform distibution. After that, it was dried under vacuum at room temperature.

2.3. PREPARATION OF ELECTRODE SOLUTION

36.78 mg of the prepared carbon supported platinum nanoparticle catalyst was mixed with 0.5 mL of Nafion, 0.15 mL of N,N-dimethyl formamide and 2.5 mL of deionized water and this mixture was sonicated until almost homogeneous dispersion (inky-like) was observed. Then, 50 μL of the slurry solution was dropped on a 0.7 cm-diameter of glassy carbon, and it was dried at 40°C for 20 minutes, 65°C for 20 minutes and 100°C for an hour to achieve good adhesion of the catalyst on glassy carbon. This was used as a working electrode for chemical studies [21].

2.4. DETERMINATION OF PLATINUM CONTENT IN THE CATALYSTS

The platinum content in each of catalysts was defined by inductively coupled plasma spectroscopy (ICP-OES, Leeman Lab) (Central Lab., METU).

2.5.CHARACTERIZATION TECHNIQUES

2.5.1. CYCLIC VOLTAMMETRY (CV)

Cyclic voltammetry is the most common and versatile method of all electrochemical techniques. Besides that it provides to obtain quantitative and qualitative information about electrochemical properties of redox active species, it is also simple and rapid for analyzing electrochemical behaviour of them [22-24].

In cyclic voltammetry measurements a triangular waveform potential is applied between the working electrode and the reference electrode such as SCE or Ag/AgCl and this potential is swept back-and-forth between two particular values as E_1 and E_2 (Fig. 2.1) [22-24].

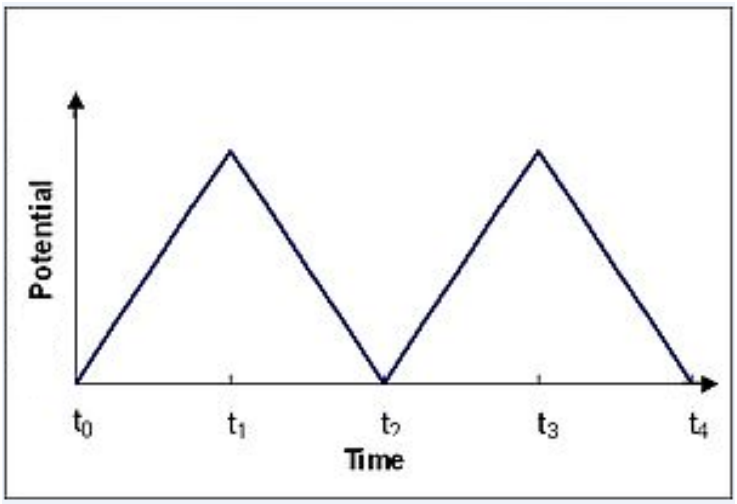

Figure 2.1. Typical cyclic voltammetry waveform signal [25].

As a result of this potential scan, the current between the working electrode and the counter electrode is recorded and the data are then plotted as current (I, vertical axis) versus potential (V, horizontal axis). When the peak occured in forward scan indicates the oxidation, the reverse scan produces the reduction peak. A representative cyclic voltammogram is given in Fig. 2.2.

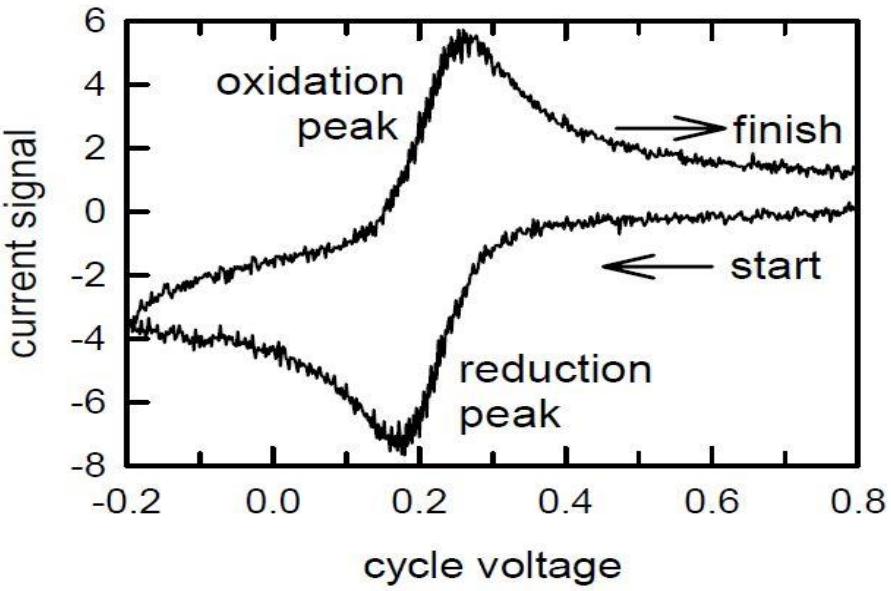

Figure 2.2. A typical cyclic voltammogram including oxidation and reduction current peaks [25].

2.5.2. CHRONOAMPEROMETRY

Chronoamperometry is a kind of electrochemical technique in which current is measured as a function of time. This technique requires a constant potential which is maintained for a defined period while the current is monitored. Single, double and even multi-step chronoamperometry can be performed in a time frame from a millisecond to hours, or even days, if it is necessary. Chronoamperometric method is widely used to interpret about long-term stabilities of electroactive species in an exact potential range. In chronoamperometric measurements, a-square waveform voltage is applied to working electrode (Figure 2.3.a.). The corresponding response of the current due to changes of the potential is shown in Figure 2.3.b. versus time [26,27].

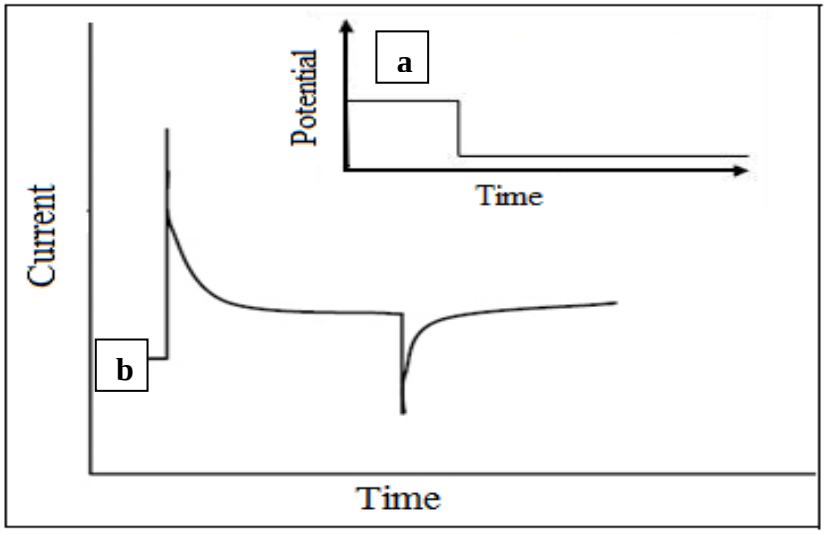

Figure 2.3. An excitation waveform signal (a) and a typical chronoamperogram (b) [26].

2.5.3. ELECTROCHEMICAL CELL DESIGN

Cyclic voltammetry (CV) and chronoamperometry (CA) measurements were carried out using a microcomputer-controlled potentiostat/galvanostat (Gamry Framework, Version 5.50, 2008) (Department of Chemistry, METU) at room temperature. In this study, a three-electrode setup was used which consists of saturated calomel electrode (SCE) as a reference electrode, glassy carbon as a counter electrode and the prepared catalysts as a working electrode. The electrolyte solution includes 0.1 M $HClO_4$ + 0.5 M CH_3OH solutions. In order to achieve working in an oxygen-free medium, Ar gas was passed through the electrolyte for ten minutes before each voltammogram was recorded [6,9,20,28].

2.5.6. X-RAY DIFFRACTION

Not only is X-ray diffraction nondestructive and powerful analytical technique but also very common method for determining crystal structure of crystallites. Moreover, XRD helps to define the mean size of crystallites and useful for fingerprint characterization. Since the discovery of X-rays by W.C. Röntgen in 1895, scientists have caught a chance to plumb the crystalline structure at the atomic level. In 1913,

W.L. Bragg & W.H. Bragg had developed a law called “Bragg’s Law” to identify the atomic structure of crystals. According to the law, the path length difference of two incident X-ray beam must have an integer value of the wavelength of incident beams:

$$2d\sin\theta = n\lambda$$

where; d is the distance between atomic layers in a crystal, θ is the angle of incident X-ray beam, n is an integer refers to the order of the diffraction peak and λ is the wavelength of the incident X-ray beam [27,29,30].

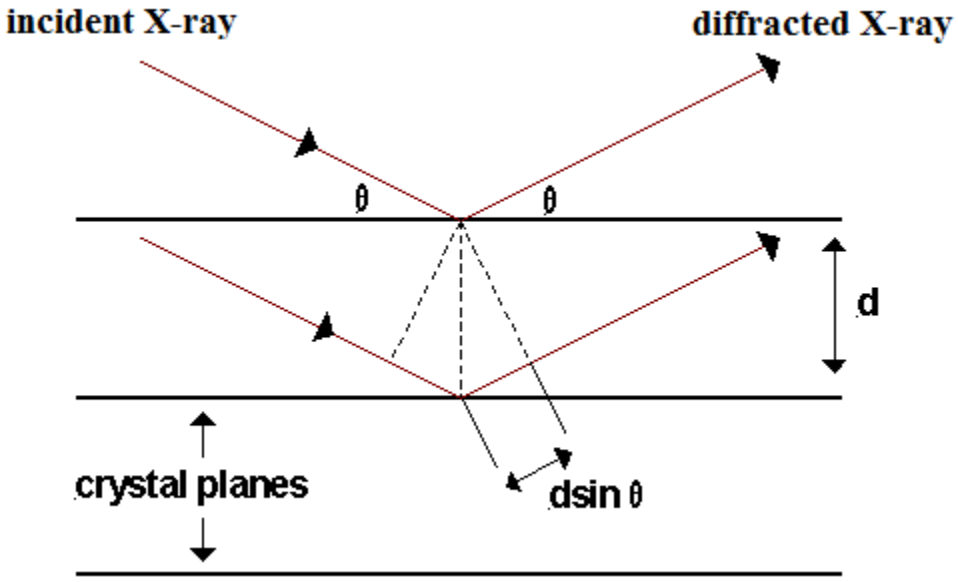

Figure 2.4. The path of X-rays [29].

As indicated earlier in this part, X-ray diffraction is also employed for identifying the particle sizes of crystallites. For this purpose, Paul Scherrer derived an equation to determine the crystallite size. From XRD peak broadening, it can be calculated with the Scherrer Equation:

$$d(Å) = k\lambda/\beta\cos\theta$$

where k is a coefficient which is taken as 0.9, λ is the wavelength of X-ray source that was used (1.54056 Å), β is the width of the peak at half of the height, θ is the position of maximum peak [6,9,29-31].

In this study, XRD measurements were performed on a Rigaku diffractometer with Miniflex + theta-theta high resolution goniometer which is equipped with a Cu Kα radiation (λ= 1.54056 Å). All the measurements were carried out at 20 kV and 30 mA. (Department of Chemistry, METU)

2.5.7. TRANSMISSION ELECTRON MICROSCOPY

Transmission electron microscopy is a widely known and versatile microscopy technique which provides atomic-resolution lattice images and chemical information at a resolution of 1 nm or better. Transmission electron microscopy runs on the same basic principles as the light microscope but uses electron beam instead of the light. In TEM electrons are used as light source, because their much lower wavelength makes it possible to get a thousand times better resolution. Moreover, TEM uses magnetic lenses to deflect electrons instead of glass lenses [32].

A schematic illustration of the microscope is shown in Figure 2.5. At the top of microscope, electrons are emitted to move through vacuum in the column of microscope. As mentioned before, in TEM electromagnetic lenses are used to focus the electrons into a very thin beam. The electron beam move through the specimen which is studied. Some electrons are scattered and disappear from the beam and that depends on the material density which is presented. At the bottom of microscope, unscattered electrons hit a fluorescent screen, which result in a shadow image of the specimen with its different parts displayed in varied darkness due to their density [32,33].

Having high density and heavier elements seem darker in the transmission electron microscopy image due to the scattering of electrons in the sample. The final image can be carried out directly by the operator or photographed with a camera. The data

recording system tends to be digital with the use of a charge coupled device (CCD), allowing quantitative data processing and quantification.

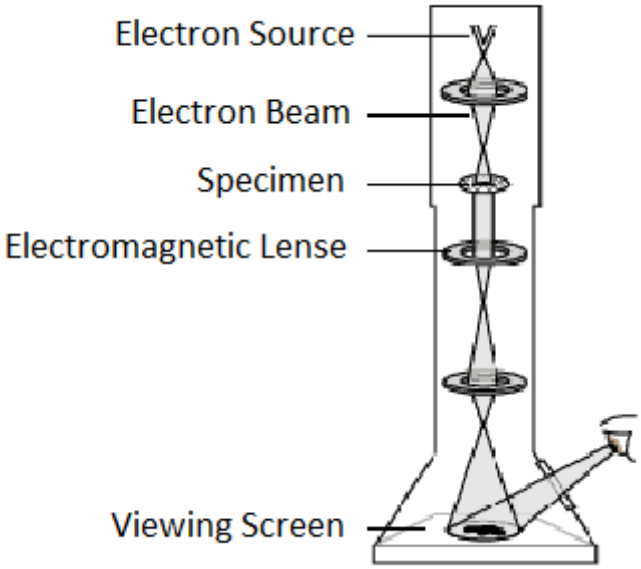

Figure 2.5. A schematic representation of a transmission electron microscope [34].

A JEOL-200 kV TEM instrument was used to obtain transmission electron microscop images. By the help of TEM images, the individual platinum nanoparticle sizes were determined and distribution of particles on carbon support was also observed. All the samples were prepared by dissolving catalyst in dry ethanol at ultrasonic bath. To get uniform dispersion, the mixtures were sonicated for hours. A drop of (~0.5 mg/mL) each suspension were placed on a 400-mesh carbon-coated copper grid and the solvent was allowed for evaporation prior to TEM analysis (Central Lab., METU).

2.5.8. X-RAY PHOTOELECTRON SPECTROSCOPY (XPS)

X-ray photoelectron spectroscopy (XPS) which is also entitled as ESCA (Electron Spectroscopy for Chemical Analysis) is the most widely used technique for surface analysis due to its relative simplicity in use and data interpretation. XPS was developed in the 1960s by Kai Siegbahn and hisi research team at University of

Uppsala, Sweden and with the demand for equipment in laboratories, Siegbahn was awarded the Nobel Prize for Physics for his work with XPS in 1981 [35,36].

From the kinetic energies of these ejected photoelectrons chemical composition of the sample can be investigated directly. Besides the specification of elements on the surface and surface composition, local chemical environments and oxidation states of transition metals can be obtained by using XPS. After we identify the elements, relative concentrations of these are determined by using the photoelectron intensities. Moreover, XPS data give information about chemical states from the variations in binding energies, or chemical shifts of photoelectron lines [35,36].

X-ray photoelectron spectroscopy works by irradiating the sample with a monochromatic and soft X-rays that causes core electrons to be ejected from the surface of sample and the energies of the emmited photoelectrons which are characteristic of the elements is measured by an electron analyzer. In Figure 2.6 the emission of photoelectrons was illustrated.

From the binding energy and intensity of a photoelectron peak, the elemental composition and chemical state of elements are determined as mentioned before. The binding energy of each of the emitted electrons can be calculated by using a formula based on the work of Ernest Rutherford:

$$E_{binding} = E_{photon} - (E_{kinetic} + \varphi)$$

Where $E_{binding}$ is binding energy of emitted electrons, E_{photon} is the energy of incident X-ray that is used, $E_{kinetic}$ is the kinetic energy of electron that is measured by the instrument and φ is the work function of the spectrometer [35,36].

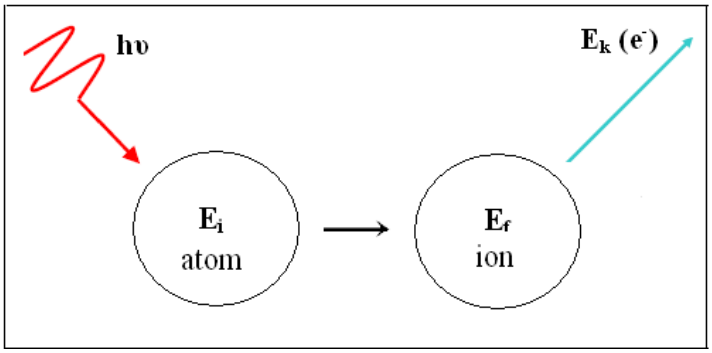

Figure 2.6. Illustration for the derivation of binding energy where E_k is the kinetic energy of the photoelectrons, E_i is the initial state and E_f is the final state [36].

In this study, a SPECS spectrometer was employed to acquaire oxidation states of platinum and determine their ratios by using Ka lines of Mg (1253.6 eV, 10 mA) as X-ray source (Central Lab., METU). XPS peaks of all platinum nanoparticles were fitted by applying a Gaussian-Lorentzian function and the C 1s line at 284.6 eV was used as reference point.

2.5.9. BRANAUER-EMMETT-TELLER (BET) SURFACE AREA ANALYSIS

BET theory is a rule for the physical adsorption of gas molecules on a solid surface and specific surface area of a material is determined by BET. The theme of the theory that it is for monolayer molecular adsorption, to multilayer adsorption with the following hypotheses:

- gas molecules physically adsorb on a solid in layers infinitely,
- no interaction occurs between layers,
- Langmuir theory can be performed to each layer.

The final BET equation is expressed by:

$$\frac{1}{\left[V_a\left(\frac{P_0}{P}-1\right)\right]}=\frac{C-1}{V_m C}\times\frac{P}{P_0}+\frac{1}{V_m C}$$

where P and P_0 are the equilibrium and the saturation pressure of adsorbates at the temperature of adsorption (in pascals), V_a is the volume of gas adsorbed at standard temperature and pressure (STP) [273.15 K and atmospheric pressure (1.013×10^5 Pa)] (in milliliters), V_m is the volume of gas adsorbed at STP to produce an apparent monolayer on the sample surface (in milliliters) and C is the BET constant that is related to the enthalpy of adsorption of the adsorbate gas on the powder sample [37].

2.5.10. FOURIER TRANSFORM INFRARED (FTIR) SPECTROSCOPY

In FTIR, spectra are obtained due to the measurements of the coherence of a radiative source, utilizing time-domain or space-domain measurements of any radiation. An infrared spectrum indicates a fingerprint of a sample with absorption peaks that correspond to vibration frequencies between atomic bonds. Because each different material has unique atom combinations, any of two compounds can't produce the exact infrared spectrum. Thus, infrared spectroscopy provides a positive identifying for all types of material. Moreover, size of the peaks in spectrum is a direct sign of the amount of species. With new software algorithms, infrared is a perfect technique for quantitative analysis. An illustration of FTIR analysis of a sample is shown in Figure 2.7. In infrared spectroscopy analysis, IR radiation is sent to a sample. Some of IR radiation is absorbed by the sample and rest of it is transmitted. The final spectrum represents the molecular absorption and transmission, creating a molecular fingerprint of the sample. Like a fingerprint no two unique molecular structures produce the same infrared spectrum [38].

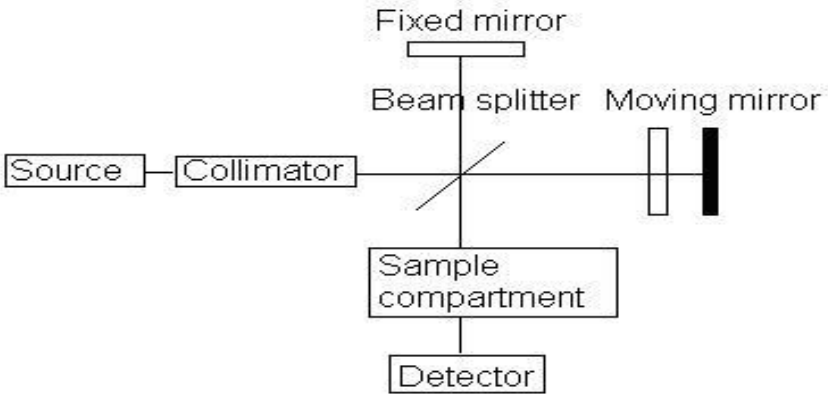

Figure 2.7. Block diagram of an FTIR spectrometer [39].

CHAPTER 3

RESULTS & DISCUSSION

3.1. X-RAY DIFFRACTION AND TRANSMISSION ELECTRON MICROSCOPY

XRD (x-ray diffraction) technique was used to define crystalline structure and average crystallite size of platinum found in catalysts. XRD pattern of all catalysts included the peaks at 39.90, 46.65, 67.55 ve 81.25 two theta corresponding to (111), (200), (220) and (311) planes of platinum, indicating that platinum has face-centered cubic (fcc) structure, Figure 3.1. XRD peak position and width data were used in Scherrer equation to calculate average crystallite size of platinum;

$$d(Å) = k\lambda/\beta\cos\theta$$

where d is the average particle size, k is Scherrer constant (0.9), λ is the wavelength of incident x-ray (1.54056 Å), β is full width half - maximum of peak (in rad) and θ is the angle of peak at maximum point [30].

In this study, the Pt (220) plane's peak data were used to calculate average particle sizes of platinum and the sizes were found to be ~5.2, ~5.2, ~5.3 ve ~ 5.3 nm for catalyst Ia, Ib, IIa, and IIb, respectively. Previous studies indicated that the average particle size of platinum crystallite changes between 1-3 nm when thiol derivatives and superhydride were used as surfactant and reducing agent, respectively [35,36]. Obviously, our results indicated that there is no much platinum particle size difference between the catalysts. However, the point should be kept in mind is that if there is a large particle size distibution among the particles, XRD is not a perfect technique to define average particle size of crystallite. Therefore, to verify these data transition electron microscopy (TEM) results should also be considered.

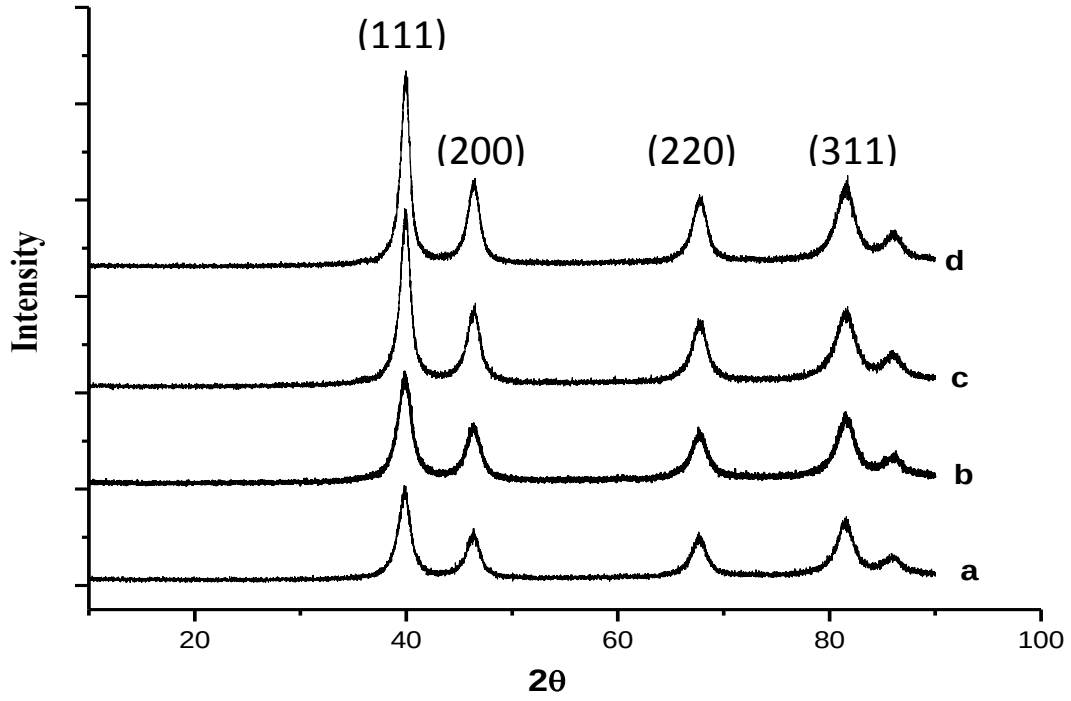

Figure 3.1. XRD of catalyst Ia (a), Ib (b), IIa (c) and IIb (d).

An individual and average particle size of platinum were determined by using TEM. It was found that all catalysts composed of small and agglomerated platinum particles but in different shape, density and ratio. For each catalyst ~200 particles from 6 or 7 different regions were examined to obtain average particle size and to plot size distribution histogram of platinum, Figure 3.2. When only the small particles were considered, the average particle sizes of Pt were found to be ~5.4, ~5.3, ~5.3 and ~5.4 for catalyst Ia, Ib, IIa and IIb, respectively. They are in good agreement with the sizes calculated by XRD data, Table 3.1. The number of small particles is larger in catalyst I compared to catalyst II and so it can be expected that the surface area of catalyst I is larger than catalyst II. Beside size, the shape of small particles were also investigated and noticed that when sodium borohydride was used as a reducing agent, mostly cubic Pt nanoparticles were obtained, Figure 3.3.a-b. On the other hand, formless Pt nanoparticles were detected when formaldehyde was used, Figure 3.3.c-d.

As pointed out above, in addition to small particles, the large (agglomerated) particles were obtained for all catalysts. These agglomerated particles were formed by combination of small particles. The shape of agglomerated particles for catalyst

Ia-b was not perfect spherical shape, but it is still possible to find rough size of these large particles and it is between 30-70 nm. It should also be stressed that the density of these particles is quite low, for instance in some case it is possible to obtain thin layers of Pt nanoparticles within agglomerated particles. This type of arrangement of metal nanoparticles causes to have large surface area of platinum catalyst as obtained from BET analysis; it is ~50 m^2/g of sample. BET measurements were done before addition of carbon support to platinum nanoparticles which consists of ~90 % of platinum and ~10 % of hydrocarbon. On the other hand, most of the particles are large (40-120 nm), dense and spherical in catalyst IIa-b, Figure 3.2.c-d. As expected, they have smaller surface area, ~22 m^2/g sample, compared to catalyst Ia and Ib.

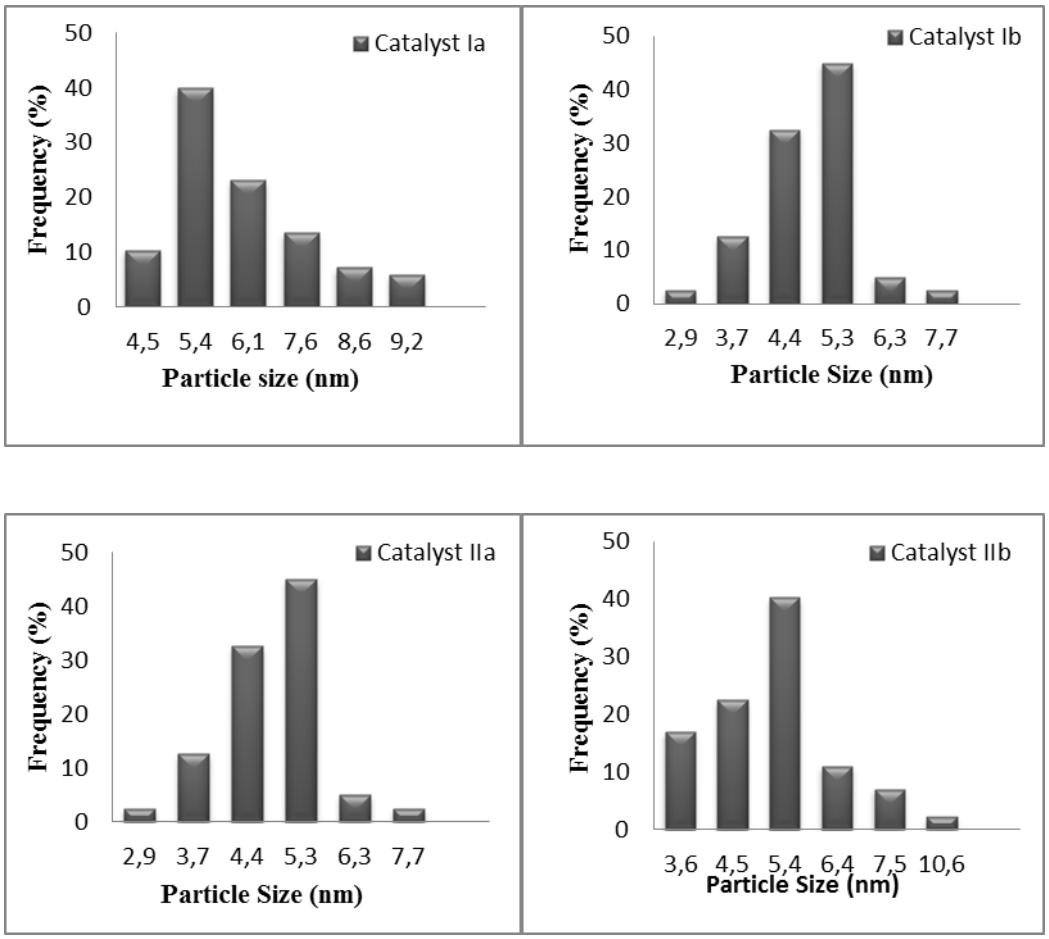

Figure 3.2. The size distribution histograms of nanoparticles in all catalysts.

Table 3.1. Average particles size determined by (a) XPS, (b) TEM.

Catalysts	**a (nm)**	**b (nm)**
Catalyst Ia	~5.2	~ 5.4
Catalyst Ib	~5.2	~ 5.3
Catalyst IIa	~5.3	~ 5.3
Catalyst IIb	~5.3	~ 5.4

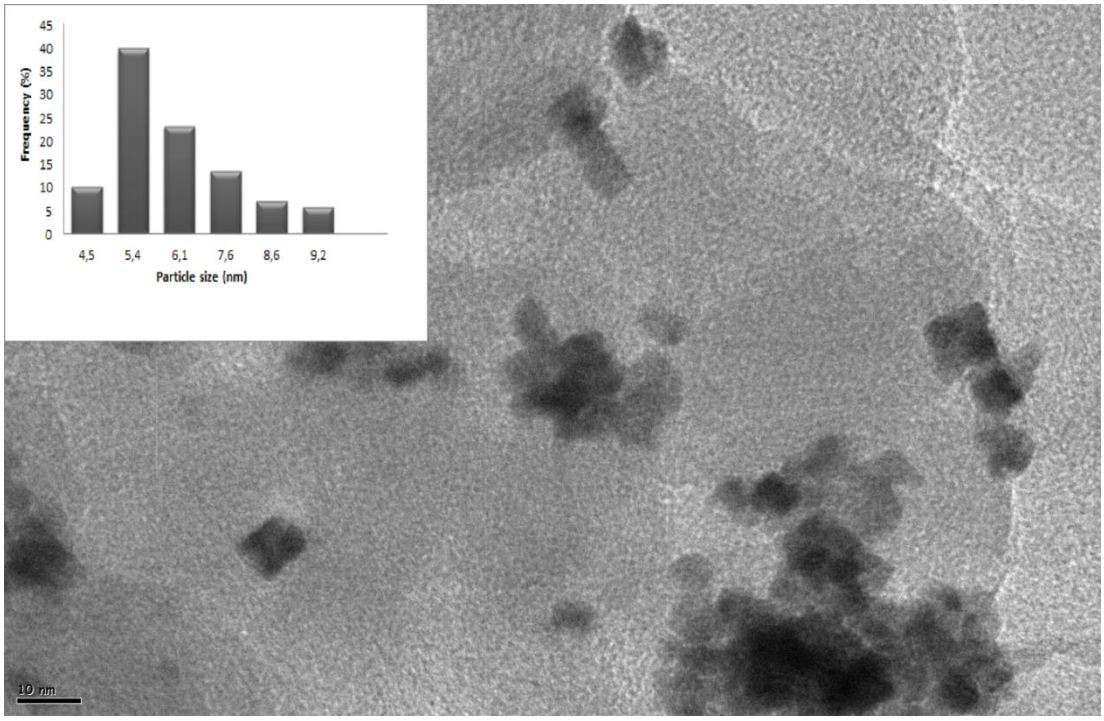

Figure 3.3.a. Transmission electron micrograph and histogram of the platinum particle size distribution of catalyst Ia.

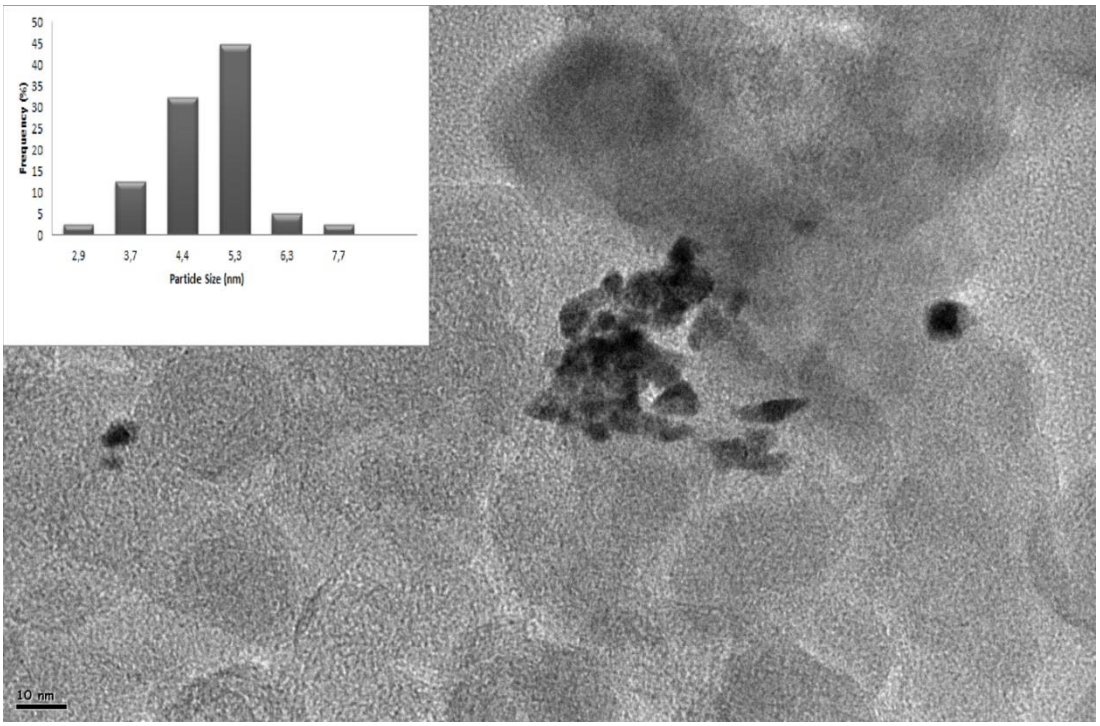

Figure 3.3.b. Transmission electron micrograph and histogram of the platinum particle size distribution of catalyst Ib.

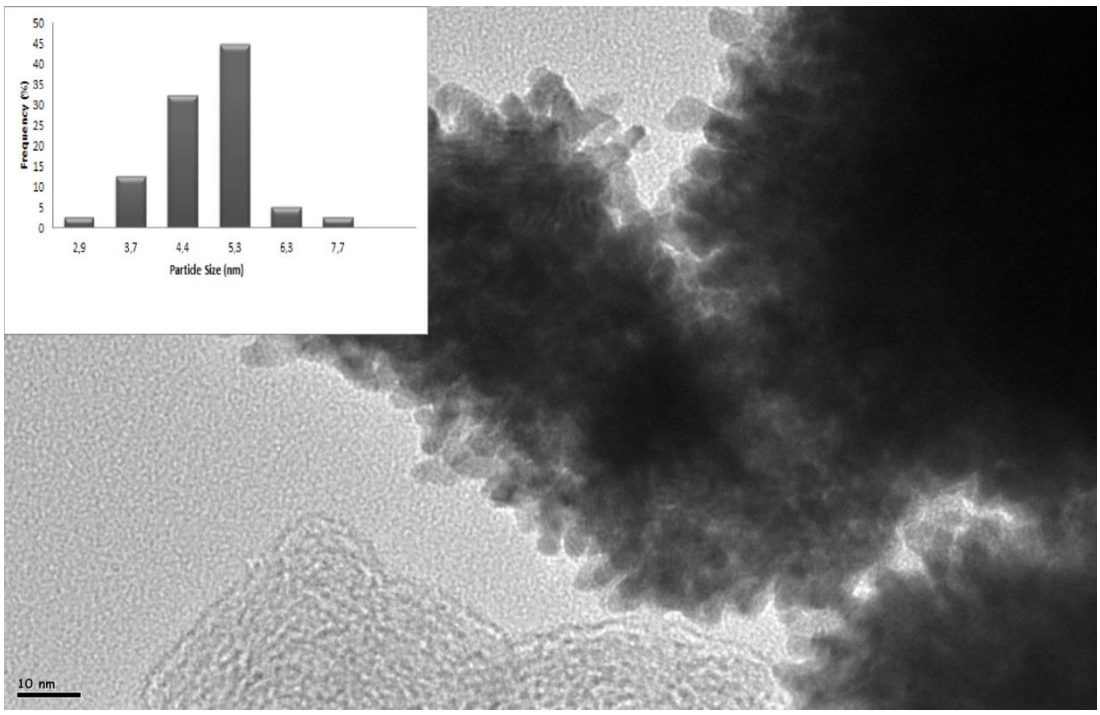

Figure 3.3.c. Transmission electron micrograph and histogram of the platinum particle size distribution of catalyst IIa.

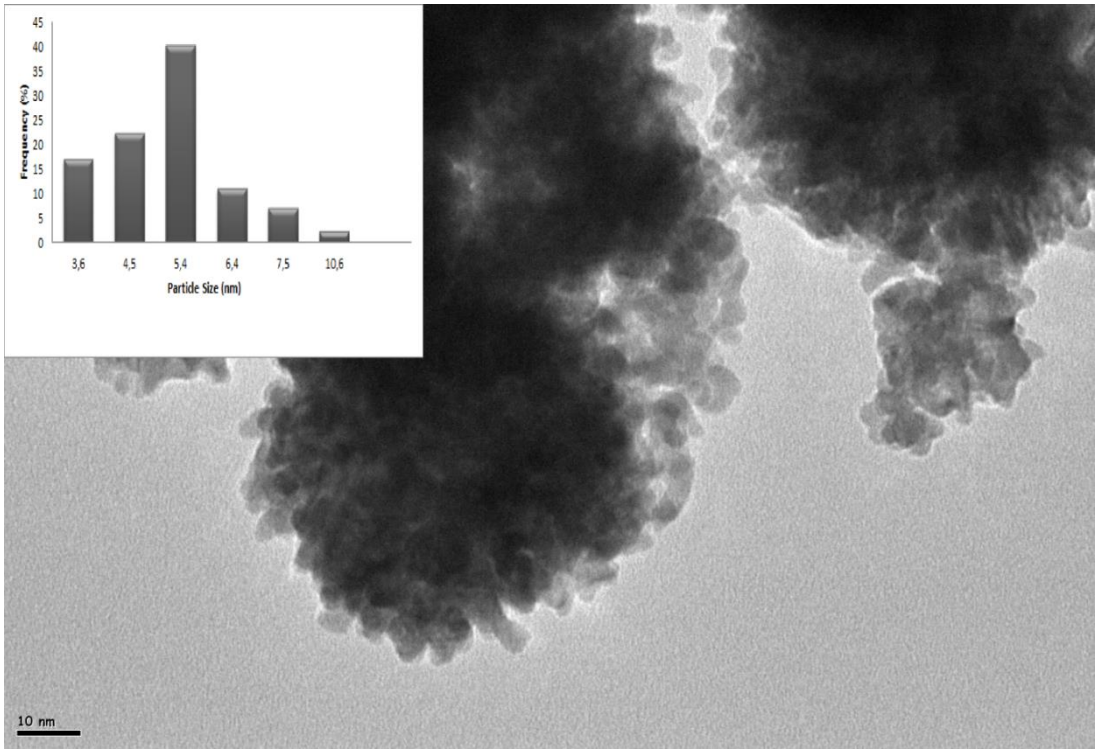

Figure 3.3.d. Transmission electron micrograph and histogram of the platinum particle size distribution of catalyst IIb.

3.2. X-RAY PHOTOELECTRON SPECTROSCOPY

In order to investigate oxidation state of elements and their ratios XPS was performed. The Pt 4f, O 1s and C 1s regions of spectra were analyzed by Gaussian-Lorentzian peak fitting programme, and C 1s peak at 284.6 eV was considered as a reference point. The evolution of Pt 4f peak was acvhieved by keeping in mind that the intensity ratio of doublet should be about 3:4 and the distance between them is ~3.3 eV [28,40]. The peak fitting studies revealed that the Pt 4f peak consists of two doublets, one at 71.0-71.3 eV and 74.2-74.5 eV, and the other one at 74.3-74.6 eV and 77.6-77.8 eV, Figure 3.4. The first doublet represents Pt(0) and the second one refers to Pt(IV) such as PtO_2, $Pt(OH)_2$ and/or $Pt(OH)_4$. There is not much peak position shift between the catalysts.

The relative amounts of Pt(0) and Pt(IV) were determined by integrating the area under each doublet and the results were presented in Table 3.2. According to the table, major amount of platinum exists as Pt(0), 65 %, and considerable amount remains as Pt(IV) oxidation state.

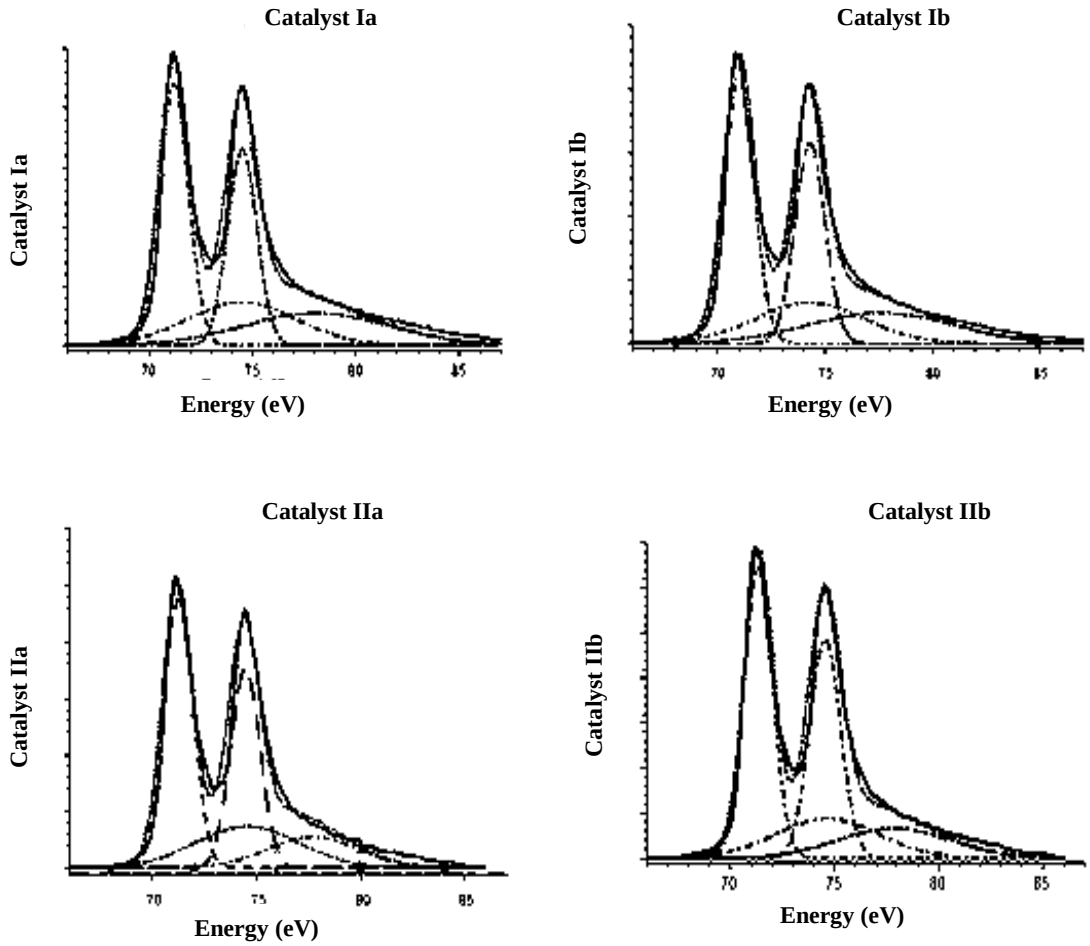

Figure 3.4. Pt 4f electron spectra of all catalysts.

In addition to Pt 4f region at spectra, the O 1s region was also examined and found out that it consisted of two singlet. The first singlet was at ~531.6 eV and the second one at 532.8 eV, Figure 3.5a-b. Previous studies indicated that the peak at 531.6 eV could be due to adsorbed OH (HO_{ads}) and/or adsorbed CO (CO_{ads}), and the peak at 532.8 eV was assigned to adsorbed water (H_2O_{ads}) on the surface of samples which

do not include carbon support. While catalyst I has ~13 % adsorbed water, catalyst II has ~26 %. It was thought that the reducing agent is an important parameter to define the kind of adsorbed species on the surface of catalyst and there is no direct relationship between the amount of adsorbed species and surfactants.

Besides Pt 4f and O 1s peaks, C 1s spectra was also evaluated. It was found that all catalyst has three kinds of carbon: a) sp^2 carbon atoms (C=C) in partially crystalline carbon (284.3 eV), b) carbon in carbonyl, C=O, (287.1 eV) and c) carbon in carboxyl, COO^-, (288.5-289 eV) [41].

Table 3.2. Pt $4f_{7/2}$, O 1s and C 1s core binding energies in eV and the relative intensities of species.

Catalysts	**Pt $4f_{7/2}$**	**Pt $4f_{7/2}$**	**O 1s**	**O 1s**	**C 1s**	**C 1s**	**C 1s**
	Pt (0)	**Pt(IV)**	**COads (HOads)**	**H_2Oads**	**C=C**	**C=O**	**$[O-C=O]^-$**
Catalyst Ia	71.2 (67.1)	74.6 (32.9)	531.6 (85.8)	532.8 (14.2)	284.3 (57.7)	286.8 (25.7)	288.4 (16.6)
Catalyst Ib	71.0 (65.7)	74.3 (34.3)	531.5 (89.0)	532.8 (11.0)	284.3 (67.9)	286.8 (19.6)	287.5 (12.5)
Catalyst IIa	71.2 (62.4)	74.4 (37.6)	531.6 (78.1)	532.8 (21.9)	284.3 (70.2)	286.9 (24.4)	288.8 (5.4)
Catalyst IIb	71.3 (61.5)	74.5 (38.5)	531.6 (70.8)	532.8 (29.2)	284.3 (51.5)	287.1 (39.9)	289.1 (8.6)

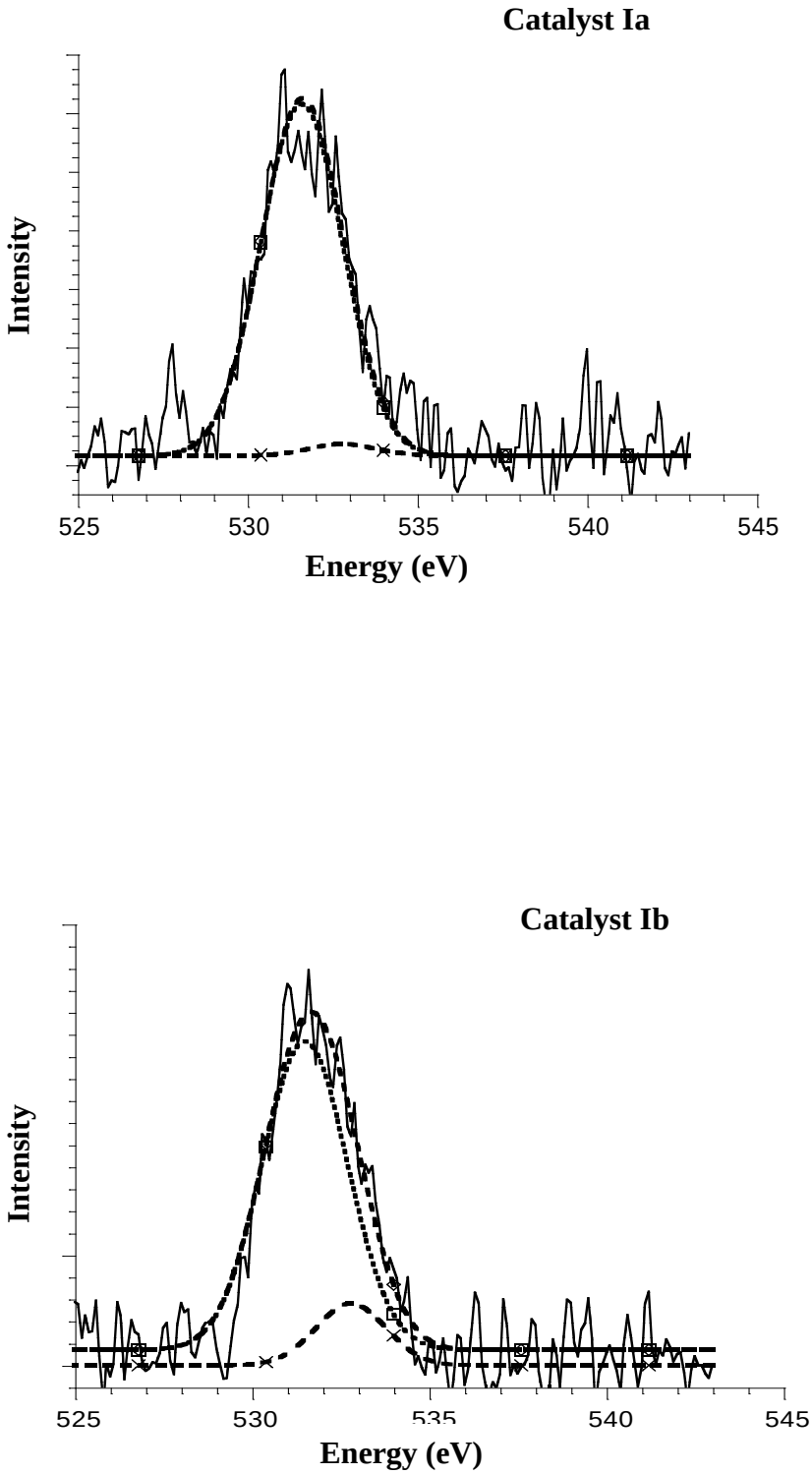

Figure 3.5.a O 1s electron spectra of catalyst Ia and Ib.

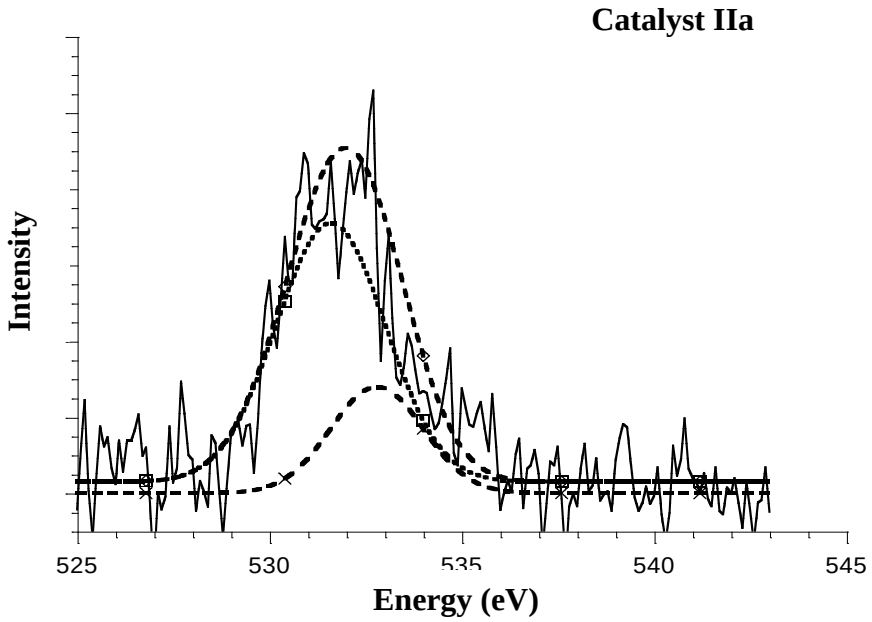

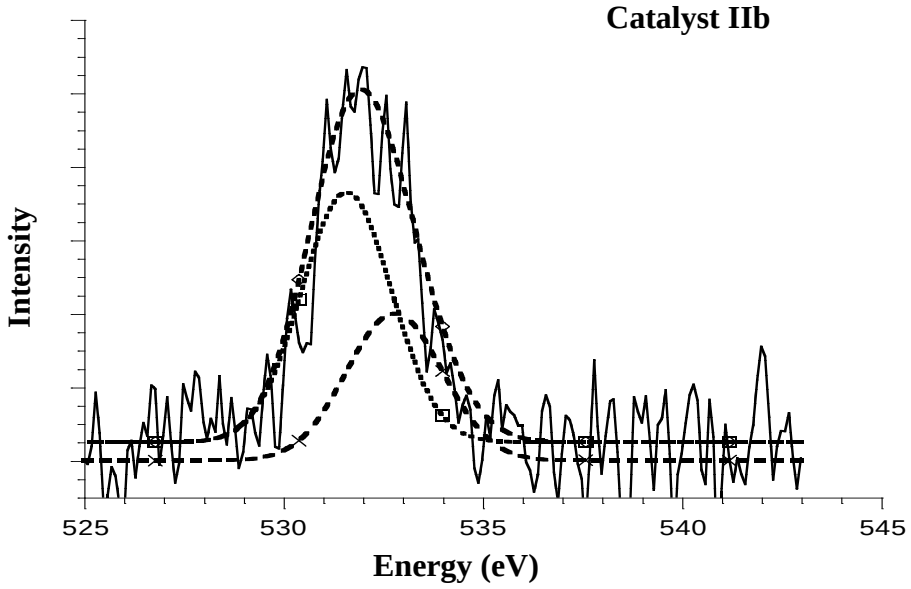

Figure 3.5.b O 1s electron spectra of catalyst IIa and IIb.

3.3. INDUCED COUPLED PLASMA SPECTROSCOPY AND BET

Induced Coupled Plasma Spectroscopy (ICP) measurements were performed to determine the platinum content of sample before adding carbon support. The results indicated that the samples were composed of ~90 % Pt and ~10 % residue coming from unremoved surfactants and/or reducing agent during washing process, Table 3.3. As can be seen from the table, catalyst I has higher surface area, ~49 m^2/g, compared to catalyst II, ~32 m^2/g (Figure 3.6.). This large difference between the surface area can be explained by TEM results. As given in XRD and TEM section, catalyst I consists of large number of small (~5 nm) particles and less dense agglomerated (30-70 nm) particles, while catalyst II compose of few number of small (~5 nm) particles, and dense and large (40-120 nm) particles.

Table 3.3. The content of platinum and the total surface area of all prepared catalysts.

Catalysts	**Pt%**	**Surface area (m^2/g)**
Catalyst Ia	89.9 ± 0.8	49.57
Catalyst Ib	89.3 ± 0.4	47.89
Catalyst IIa	91.3 ± 0.6	34.62
Catalyst IIb	89.6±0.8	30.27

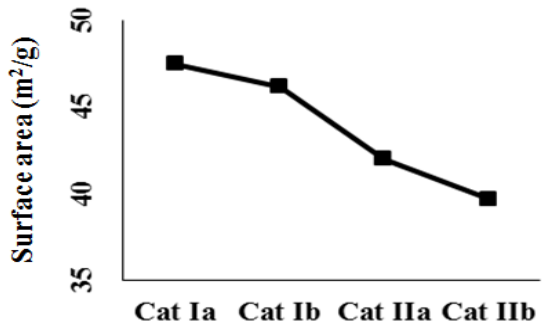

Figure 3.6. Electrochemical surface area versus catalysts.

3.4. CYCLIC VOLTAMMETRY AND CHRONOAMPEROMETRY

The electrochemical properties and performance of catalysts towards methanol oxidation reaction were determined by using cyclic voltammogram and chronoamperometry. First, CV measurements were done in 0.1 M $HClO_4$ at room temperature with a scan of 50 mV/sec. Similar CV's were obtained for all catalysts and the CV of catalyst Ia was given as an example, Figure 3.7. Typical hydrogen adsorption/desorption peaks were observed on the left, and oxygen evolution and reduction of Pt-oxide and/or Pt-hydroxide to platinum peaks were detected on the right and middle of the voltammogram [6]. Then, methanol was added to the electrolyte solution to form 0.5 M CH_3OH + 0.1 M $HClO_4$ reaction medium. The pattern of voltammogram was changed dramatically, Figure 3.8. Methanol oxidation begins at ~0.35 V on anodic scan and reachs maximum at ~0.8 V and incompletely oxidized intermediate species such as CO starts to remove from the surface of catalyst at ~0.7 V and reach maximum at ~0.55 V in the reverse scan.

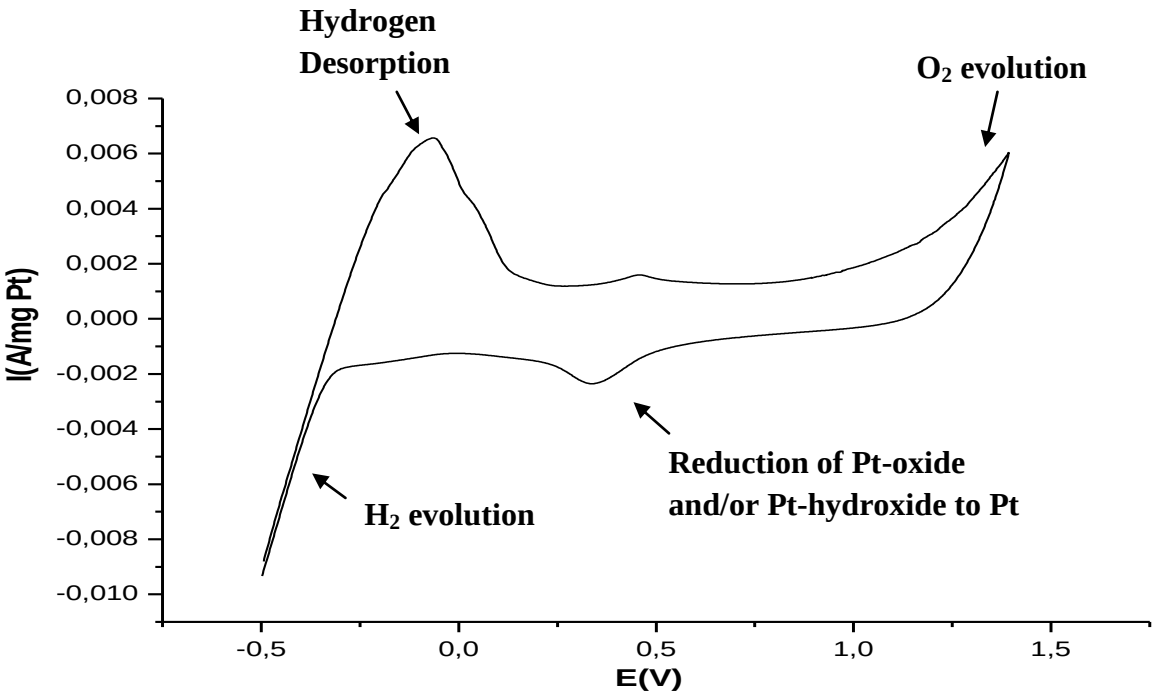

Figure 3.7. Cyclic voltammogram of catalyst Ia in 0.1 M $HClO_4$ at room temperature

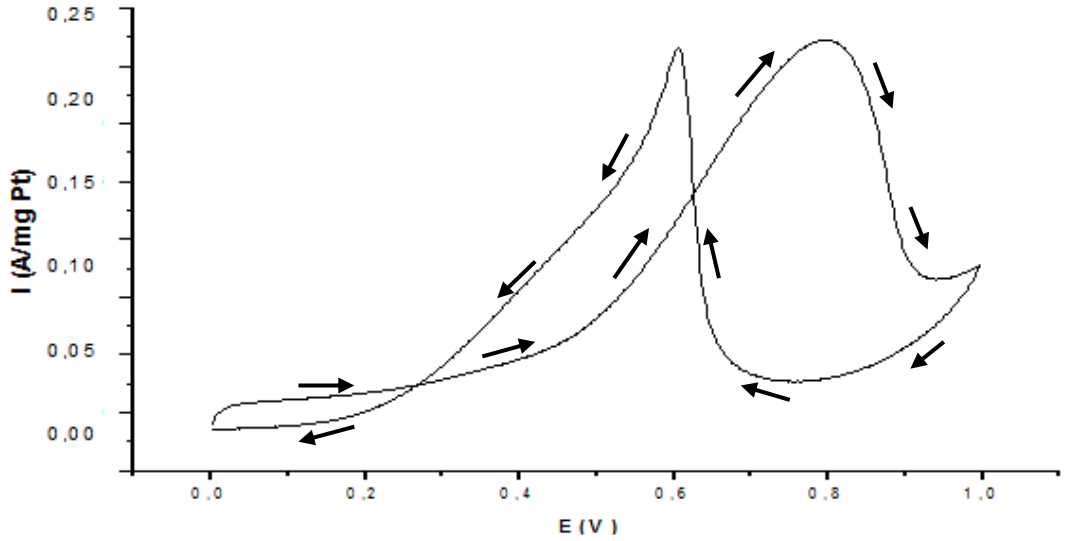

Figure 3.8. Cyclic voltammogram of catalyst Ia in 0.1 M $HClO_4$ + 0.5 M CH_3OH at room temperature.

To compare the performance of catalysts easily, only the anodic part of the CV's were recorded and given in Figure 3.9. There are several parameters to define the performance of catalysts such as; a) on-set potential, b) peak potential, c) current density and d) I_f/I_r ratio for methanol oxidation reaction. It is well known that the lower the on-set and peak potential, the higher the I_f/I_r ratio and current density, the better the performance of the catalyst. Figure 3.9 and Table 3.4 results displayed that catalyst I and catalyst a have greater I_f/I_r ratio compared to catalyst II and catalyst b, respectively, indicating that both reducing agents and surfactants effect the performance of the catalysts. Under these circumstances, catalyst Ia has the highest current density (240 mA/mg), I_f/I_r ratio (1.13), Table 3.4. The order of the current density is catalyst Ia>Ib>IIa>IIb.

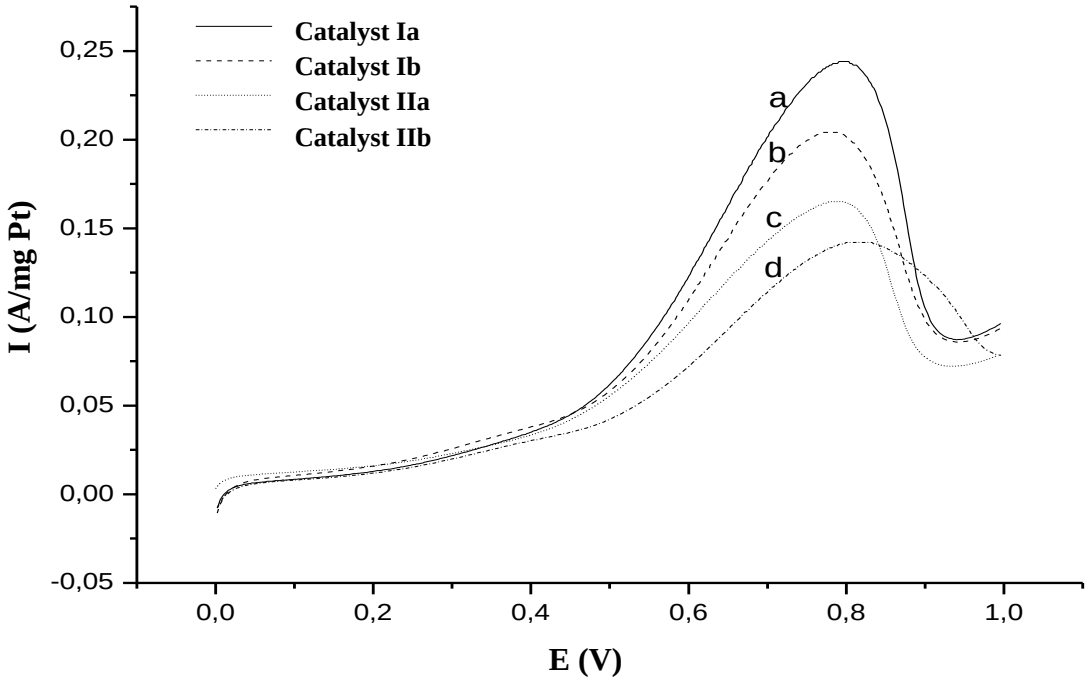

Figure 3.9. Anodic part of cyclic voltammogram of catalyst Ia (a), Ib (b), IIa (c), IIb (d) in 0.1 M $HClO_4$ + 0.5M CH_3OH at room temperature (50 mV/sec).

Table 3.4. The peak potential and current density at peak, and I_f/I_r for methanol oxidation reaction.

Catalysts	**Peak potential (V)**	**Current (mA/mg Pt)**	**I_f/I_r**
Catalyst Ia	0.80	240	1.13
Catalyst Ib	0.80	210	1.08
Catalyst IIa	0.80	170	0.97
Catalyst IIb	0.81	140	0.94

To define long-term stability of all catalysts chronoamperometry analysis was carried out in a mixture of 0.1 M $HClO_4$ + 0.5M CH_3OH at room temperature by applying constant potential (~0.8 V) for 3600 s. The results were illustrated in Figure 3.10. All the catalyst started with high current and then decreased slowly. According to this results, the order of maximum currents were found as catalyst Ia>Ib>IIa>IIb, respectively. This order and also the current values were compatible with CV results.

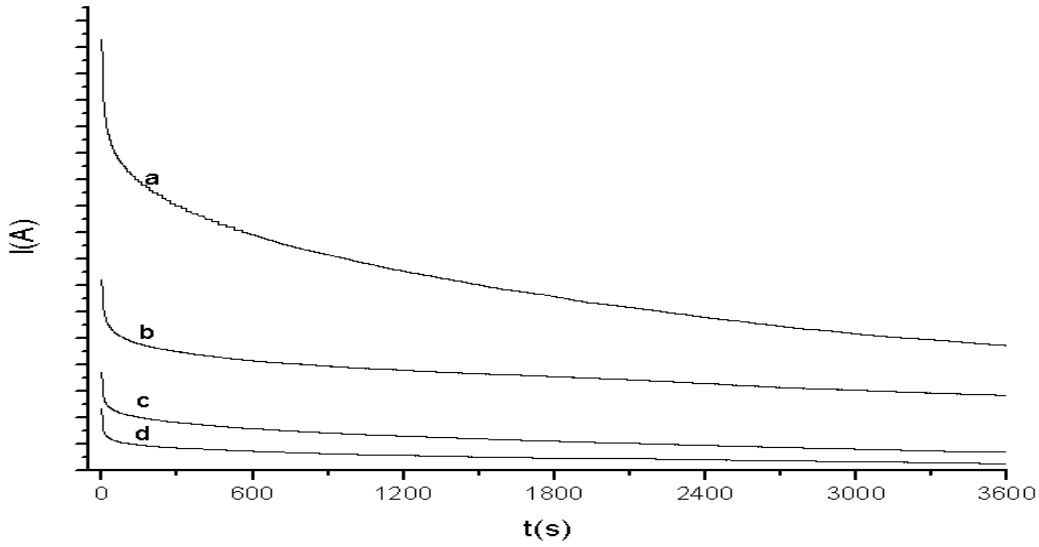

Figure 3.10. Chronoamperometric curves of catalyst Ia (a), Ib (b), IIa (c) and IIb (d) in 0.1 M $HClO_4$ + 0.5M CH_3OH at room temperature.

In order to clarify the causes behind performance of catalysts, chemical surface area (CSA), electrochemical surface area (ECSA), percent platinum utility and roughness factor (RF) for each catalyst have been calculated and given in Table 3.5. The chemical surface area of platinum was determined by using following formula [20]:

$$CSA\ (m^2/g\ Pt) = 6000 / (\rho \times d)$$

where ρ is the average density of platinum (21.4 g/cm^3) and d is the mean diameter of platinum crystalline particles in nm. It is difficult to define the exact diameter of Pt nanoparticles, because they consist of small and agglomerated particles, therefore

to estimate CSA, only the mean diameter of small Pt nanoparticles were considered and calculations using XRD and TEM results indicated that CSA of all catalysts are ~53.0 m^2/g Pt.

Electrochemical surface area (ECSA) of platinum was calculated by using CV data, and the formula is given below [20]:

$$ECSA\ (cm^2/g\ Pt) = Q_{hyd}\ (mC) / (a.b)$$

where Q is the charge (mC/cm^2 Pt) calculated from hydrogen desorption region, a is the constant (0.21 mC/cm^2), and b is the amount of platinum in g/cm^2 electrode. The average ECSA was found to be ~47.0 and 41.0 m^2/g Pt for catalyst I and catalyst II, respectively (Table 3.5). It is not possible to find a direct relationship between ECSA and the kind of surfactant, but reducing agent. The catalysts prepared by sodium borohydride have higher ECSA than the catalysts prepared by formaldehyde.

Table 3.5. CSA and % platinum utility found from TEM and XRD data, ECSA and roughness factor (RF) for all the prepared catalysts.

Catalysts	**CSA (m^2/gPt) (TEM, a)**	**CSA (m^2/gPt) (XRD, b)**	**|a-b|**	**ECSA (m^2/g Pt)**	**% Pt utility (TEM) (c)**	**% Pt utility (XRD) (d)**	**|c-d|**	**RF**
Catalyst Ia	51.9	53.2	1.3	47.5	91.5	89.2	2.3	73.2
Catalyst Ib	52.9	53.2	0.3	46.2	87.3	86.9	0.4	71.0
Catalyst IIa	52.9	52.9	0	42.0	79.4	79.4	0	64.5
Catalyst IIb	51.9	52.9	1.0	39.7	76.5	75.1	1.4	61.0

The percent platinum utility (1) and roughness factor (2) of each catalyst were calculated from following formulas [20]:

$$\text{Pt \% utility} = (\text{ECSA/CSA}) \times 100 \qquad (1)$$

$$\text{RF} = \text{A real area / A geometrical area} \qquad (2)$$

where a real area= Q_{hyd} (mC)/(0.21 mC/cm^2 Pt) and a geometrical area= $\pi.r^2$= 0.38 cm^2 (r is the radius of electrode, 0.35 cm). Percent platinum utility and roughness factor's of catalyst I and catalyst a are larger than catalyst II and catalyst b, respectively, and the highest value was obtained for catalyst Ia, which is in good aggreement with the performance of the catalyst.

3.4. FOURIER TRANSFORM INFRARED SPECTROSCOPY

The FTIR spectra of all the prepared catalysts were analyzed to get information about the species in catalysts. Sample pellets were prepared by mixing sample without carbon support 1% KBr. The spectra of catalysts, propylamine, dipropylamine and carbon XC-72 were illustrated in Figure 3.11.

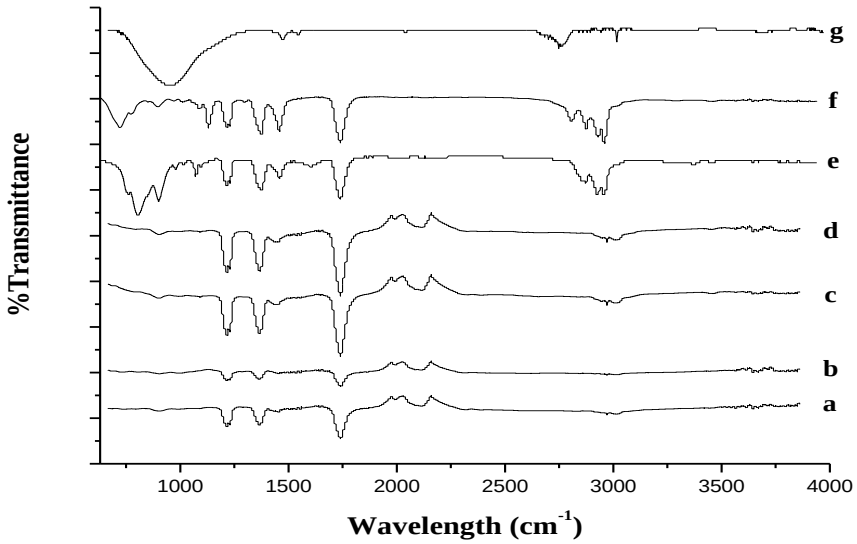

Figure 3.11. FTIR spectra of propylamine (a), catalyst Ia (b), catalyst IIa (c), dipropylamine (d), catalyst Ib (e), catalyst IIb (f).

As can be seen from the figure, FTIR spectra of all catalysts showed the same pattern, but they are different than surfactants (propylamine and dipropylamine) and carbon XC-72, indicating that the surfactants were decompose during preparation and same type of hydrocarbon were formed around platinum nanoparticles. Moreover, possible species seen in Figure 3.11 are shown in Table 3.6.

Table 3.6. Possible species on platinum catalysts.

Freguency ($cm^{-1)}$	**Bond**
2140-1990	C-N bond (any)
1720-1740	C=O stretch (aldehydes)
1760–1690	C=O stretch (carboxylic acids)
1320–1000	C–O stretch (alcohols)
1370–1350	C–H rock (alkanes)
1470–1450	C–H bend (alkanes)
2099-2091	Pt^0-CO band
1500-1300	adsorbed COOH

CHAPTER IV

CONCLUSION

In this study, carbon supported platinum nanoparticles catalysts were prepared by using $PtCl_4$ as precursor, sodium borohydride and formaldehyde as reducing agent, and propylamine and dipropylamine as surfactant. XRD, TEM, XPS, ICP, BET, CV and CA results indicated that:

a) Platinum crystallized in the form of face-centered cubic (fcc) structure,

b) Cubic and formless platinum nanoparticles were observed for catalyst I and catalyst II, respectively.

c) All catalysts composed of small and agglomerated particles in different morphology and ratio, for instance; catalyst I contains large number of small (~5 nm) and few number of agglomerated and less dense platinum particles (~30-70 nm), while catalyst II includes significant amount of dense agglomerated platinum particles (~40-120 nm).

d) Platinum was found to be Pt(0) and Pt(IV), and Pt(0)/Pt(IV) ratio was ~2.0 for catalyst I and ~1.6 for catalyst II.

e) The surface of platinum was covered by CO, H_2O, OH^-, COO^- and hydrocarbon.

f) The reducing agent and surfactant affect the performance of the catalyst.

g) The catalyst I showed better performance towards methanol oxidation reaction than catalyst II and the order of the catalytic performance was defined as catalyst Ia>Ib>IIa>IIb.

h) The highest catalytic performance was observed for catalyst Ia, because it has the highest electrochemical surface area, percent platinum utility and roughness factor.

i) The performance of catalyst Ia (240 mA/mg Pt) was ~3 times larger than commercial E-TEK catalyst (75 mA/mg).

REFERENCES

[1] Demirel, Y., Energy, Green Energy and Technology, DOI: 10.1007/978-1-4471-2372-9-2, Springer-Verlag London Limited, 2012.

[2] Moomaw, W., Yamba, F., Renewable Energy and Climate Change, New York, USA, 2011.

[3] Appleby J., Fuel Cell Handbook. New York: Van Reinhold Co., 1989.

[4] Li, X., Principles of Fuel Cells, Taylor & Francis Group, New York, 2006.

[5] Bagotsky, V.S., Fuel Cells: Problems and Solutions, John Wiley & Sons, Inc., New Jersey, 2009.

[6] Şen, S., Activity of Carbon Supported Platinum Nanoparticles Toward Methanol Oxidation Reactions: Role of Metal Presursor and New Surfactants, Master of Science Thesis in Chemistry, METU, Ankara, 2008.

[7] Hoogers, G., Section I, Fuel Cell Technology Handbook, CRS Press LLC, Florida, 2003.

[8] Grove, W., R., On Voltaic Series and the Combination of Gases by Platinum, Philosophical Magazine and Journal of Science vol. XIV, 127–130, 1839.

[9] Gökağaç, G., Metal Oxides as Promoters for Methanol Oxidation, Doctor of Philosophy Thesis in Chemistry, University of Sydney, Australia, 1993.

[10] Aricò, A.,S., Baglio, V., and Antonucci, V., Electrocatalysis of Direct Methanol Fuel Cells, Weinheim, 2009.

[11] Mardini, S., OpenCraft Technical Seminar, 2007.

[12] Kordesch, Karl, and Günter Simader. Fuel Cells and Their Applications. New York: VCH, 1996.

[13] Noriko Hikosaka Behling, Fuel Cells: Current Technology Challenges and Future Research Needs, 2013.

[14] Carrette, L., Friedrich, K., A., Stimming, U., ChemPhysChem, 12/2000; 1(4):162–193, 2000.

[15] Arico, A.S., Baglio, V., Antonucci, V., Direct Methanol Fuel Cells, Nova Science Publishers, Inc., New York, 2010.

[16] Hosokawa,M., Nogi, K., Naito, M., Yokoyama, T., Nanoparticle Technology Handbook, Elsevier BV., Amsterdam, 2007.

[17] Guo, J.W., Zhao, T.S., Prabhuram, J., Wong, C.W., Electrochim. Acta., 50, 1973–1983, 2005.

[18] Horikoshi, S., Serpone, N., Microwaves in Nanoparticle Synthesis: Fundamentals and Applications, WILEY-VCH, Weinheim, 2013.

[19] Griffiths, P., de Hasseth, J.A, Fourier Transform Infrared Spectrometry, 2nd Edition, Wiley-Blackwell, 2007.

[20] Ertan, S., Şen, F., Şen, S., Gökağaç, G., J. Nanopart. Res., 14, 922-933, 2012.

[21] Gökağaç, G., Leger, J.M., Hahn, F., Z. Naturforsch, 56 b, 1306, 2001.

[22] Nicholson, R., S., Anal. Chem., 37 (11), 1351–1355, 1965.

[23] Kissinger, P., T., Heineman, W., R., Chem. Educ., 60 (9), 702, 1983.

[24] Mabbott G., A., J. Chem. Educ., 60 (9), 697, 1983.

[25] Öztürk, Z., Carbon Supported Platinum-Palladium Catalysts for Methanol and Ethanol Oxidation Reactions, Master of Science Thesis in Chemistry, METU, Ankara, 2011.

[26] Kissinger, P., Heineman, W., R., Laboratory Techniques in Electroanalytical Chemistry, Second Edition, Revised and Expanded (2 ed.). CRC., 1996.

[27] Bard, A., J., Faulkner, L., R., Electrochemical Methods: Fundamentals and Applications (2 ed.). Wiley, 2000.

[28] Şen, F., Şen, S., Gökağaç, G., Phys. Chem. Chem. Phys,. 13, 1676-1684, 2011.

[29] Cullity, B., D., Stock, S.,R., Elements of X-ray Diffraction, Third Edition, 2001.

[30] Scherrer, P., Nachr. Ges. Wiss. Göttingen, 26 September, 98, 1918.

[31] Antolini, E., Cardellini, F., Journal of Alloys and Compounds 315, 118–122, 2001.

[32] Williams, D., B., Carter, C. B., Transmission Electron Microscopy: A Textbook for Materials Science, Springer, New York, 2009.

[33]Reimer, L., Kohl, H., Transmission Electron Microscopy: Physics of Image Formation, Springer, New York, 2008.

[34] Egerton, R. F., Physical Principles of Electron Microscopy: An introduction to TEM, SEM, and AEM, Springer, 1st Edition, New York, 2005.

[35] Hollander, J., M., Jolly, W., L., Acc. Chem. Res., 3 (6), 193–200, 1970.

[36] Watts, J.F., Wolstenholme, J., An Introduction to Surface Analysis by XPS and AES, John Wiley and Sons, Ltd., Chichester, 2003.

[37] Brunauer, S., Emmett P. H. and Teller, E., J. Am. Chem. Soc., 60, 309, 1938.

[38] Griffiths, P., de Hasseth, J.A, Fourier Transform Infrared Spectrometry, 2nd Edition, Wiley-Blackwell, 2007.

[39] Perkins, W.D., Fourier Transform-Infrared Spectroscopy, Ed. Frank A. Settle, Jr. Journal of Chemical Education, 63:1, A5-A10, 1986.

[40] Şen, F., Gökağaç, G., Şen, S., J. Nanopart. Res.15, 1979-1988, 2013.

[41] Yang, S., Chang, K., Tien, H., Lee, Y., Li, S., Wang, Y., Wang, J., Ma, C. M., Hu, C., J. Mater. Chem., 21, 2374-2380, 2011.

[42] Fairbanks, J. W., Diesel Engine Emission Reduction Conference, Coronado, California, 2004.